Depositional history, tectonics, and provenance of the Cambrian-Ordovician boundary interval in the western margin of the North China block

Paul M. Myrow[1,†], Jitao Chen[2,§], Zachary Snyder[1], Stephen Leslie[3], David A. Fike[4], C. Mark Fanning[5], Jinliang Yuan[6], and Peng Tang[7]

[1]*Department of Geology, Colorado College, Colorado Springs, Colorado 80903, USA*
[2]*Key Laboratory of Economic Stratigraphy and Palaeogeography, Nanjing Institute of Geology and Palaeontology, Chinese Academy of Sciences, Nanjing 210008, China*
[3]*Department of Geology and Environmental Sciences, James Madison University, Harrisonburg, Virginia 22807, USA*
[4]*Department of Earth and Planetary Sciences, Washington University, St. Louis, Missouri 63130, USA*
[5]*Research School of Earth Sciences, The Australian National University, Canberra, ACT 0200, Australia*
[6]*Nanjing Institute of Geology and Palaeontology, Chinese Academy of Sciences, Nanjing 210008, China*
[7]*State Key Laboratory of Palaeobiology and Stratigraphy, Nanjing Institute of Geology and Palaeontology, Chinese Academy of Sciences, Nanjing 210008, China*

ABSTRACT

Cambrian–Ordovician strata of the North China block, one of China's main tectonic provinces, are a thick (up to 1800 m) succession of mixed carbonate and siliciclastic sedimentary rocks. Sedimentological, biostratigraphic, and chemostratigraphic analysis of strata that straddle the Cambrian-Ordovician boundary at the Subaiyingou section in the present-day western part of Inner Mongolia (northwest China) indicate the presence of a significant unconformity between mixed carbonate–fine-siliciclastic strata of the Cambrian Series 3 Abuqiehai Formation, and dominantly carbonate strata of the early Middle Ordovician Sandaokan Formation. The latter is a transgressive systems tract with retrogradationally stacked parasequences that include lowstand shoreline quartz sandstone deposits. The Abuqiehai strata have similar sedimentological characteristics to those of the Cambrian Laurentian inner detrital belt, including slightly bioturbated lime mudstone and marlstone/shale, grainstone, flat-pebble conglomerate, and microbialite. The lower part of the Sandaokan Formation records the rising limb of the middle Darriwilian positive isotopic excursion, recognized herein for the first time in the western North China block.

A Cambrian-Ordovician unconformity is developed in many successions globally, and our section in Inner Mongolia records a hiatus of similar timing and duration to a regionally extensive unconformity recorded along the ancient northern Indian continental margin. Other parts of the North China block record a hiatus of much shorter duration but show a similar record of input of siliciclastic sediment above the unconformity. We interpret the western margin of the North China block to have been affected by a regionally significant tectonic event that occurred on the northern margin of east Gondwana, the Kurgiakh or Bhimphedian orogeny. The Inner Mongolian region was, therefore, likely an along-strike continuation of the northern Indian margin, in contrast to most recent paleogeographic reconstructions.

INTRODUCTION

China's tectonic framework includes three major continental-scale cratonic masses: the North China, South China, and Tarim blocks (Meyerhoff et al., 1991; Meng et al., 1997). The North China block, also known as the Sino-Korean block, was a stable equatorial to subequatorial craton during the Cambrian (Meng et al., 1997; Huang et al., 2000; Chough et al., 2010). It covers an area ~1500 km east-west and 1000 km north-south (Fig. 1; Meng et al., 1997). It is delineated to the north by a major fault and suture zone called the Northern tectonic belt of Junggar-Hinggan, which formed during the Permian collision of the North China block with the Mongolian plate (Meng et al., 1997; Lee and Chough, 2011). The southern and southwestern borders of the block are marked by the Middle tectonic belt of Kunlun-Qilian-Qinling (Meng et al., 1997), a set of Late Ordovician to Early Silurian structures that formed during accretion of microtectonic blocks onto the southern margin of the North China block (Bian et al., 2001). The eastern margin of the block is defined by the major strike-slip Tanlu fault (Meng et al., 1997), which formed as a result of collision with South China (Lee and Chough, 2011). Some paleogeographic reconstructions show an extension of the North China block in the Korean Peninsula (e.g., Chough et al., 2000). The western margin of the block is characterized by the northeast-trending Helan aulacogen (Sun and Liu, 1983; Lin et al., 1991; Darby and Ritts, 2002).

The North China block was inundated during the Early Cambrian global transgression, forming a vast epeiric platform on which a thick (up to 1800 m) Cambrian–Ordovician succession of mixed carbonate and siliciclastic deposits accumulated (Meng et al., 1997; Chough et al., 2010). Transgression was initiated from the southeast, but the vast, relatively flat peneplain of the craton was almost simultaneously submerged except for some scattered archipelagoes (Meng et al., 1997; Lee and Chough, 2011). Fine siliciclastic sediment was sourced from these highlands and distributed by tidal currents on the seafloor in the Early Cambrian

[†]E-mail: pmyrow@coloradocollege.edu
[§]E-mail: jtchen@nigpas.ac.cn

GSA Bulletin; September/October 2015; v. 127; no. 9/10; p. 1174–1193; doi: 10.1130/B31228.1; 15 figures; 1 table; Data Repository item 2015106; published online 10 March 2015.

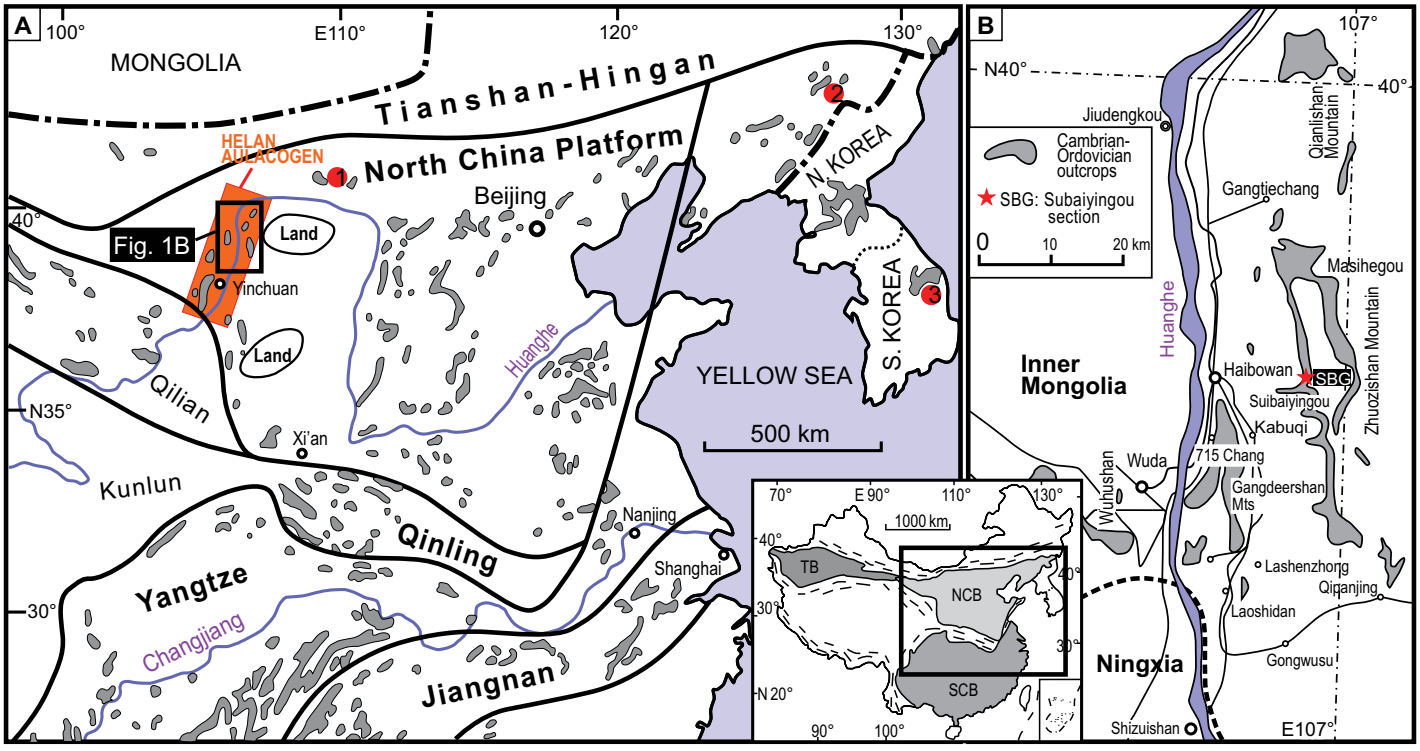

Figure 1. Simplified lithotectonic maps of mainland China (center inset) and location map of study area. (A) Location map showing lithotectonic blocks, including North China Platform, and the location of the field area in the western Inner Mongolia region. Gray areas indicate Cambrian-Ordovician outcrop exposures. Diagonal shading indicates two unsubmerged landmasses during the Late Cambrian in the western part of the North China Platform (from Meng et al., 1997). Red dots indicate reported Cambrian-Ordovician unconformities in: 1—Daqingshan Mountain region, North China; 2—Dayangcha region, Northeast China; and 3—Taebaeksan Basin, South Korea. (B) Close-up map showing location of the Subaiyingou (SBG) site in the vicinity of Haibowan.

(Lee and Chough, 2011). During the Middle to Late Cambrian, the majority of the North China block was submerged except for two main small landmasses in the west (Fig. 1; Meng et al., 1997; Feng et al., 2002). Much is known about the strata in the eastern part of the North China block with respect to sedimentary processes, paleontology, stratigraphy, and tectonic evolution (e.g., Kwon et al., 2006; Chough et al., 2010; Chen et al., 2011, 2012; Lee and Chough, 2011; Chen and Lee, 2013, 2014), but little is known of its western margin. There, a thick succession of strata was deposited in the Helan aulacogen, a tectonic feature that formed along this margin during the Mesoproterozoic, and then experienced uplift during the Neoproterozoic and renewed subsidence during the latest Neoproterozoic (Sun and Liu, 1983; Lin et al., 1991).

In the western part of the North China block, the highlands had important influences on regional sedimentological patterns and the nature of the lithofacies during the Middle to Late Cambrian and Ordovician. This is in contrast to other parts of the North China block, which had few or no exposed highlands. The eastern and northern parts of the North China block (e.g., the Shandong and Beijing regions) were entirely submerged during the Middle to Late Cambrian and Ordovician, resulting in deposition of a continuous carbonate succession (Meng et al., 1997; Chen et al., 2014). The disparities in depositional history are due, in part, to both the initial transgression being directed from the southeast (e.g., Kwon et al., 2006) and the presence of topographic complexities at the time (Meng et al., 1997). The tectonic history of the western margin of the North China block is complex due to the presence of the Helan aulacogen, which also affected sediment dispersal patterns. The stratigraphic record, including major unconformities, and the inferred tectonic history can be compared to that recorded in potentially adjacent tectonic blocks in various paleogeographic reconstructions in order to evaluate the potential placement of blocks within various tectonic models.

The present study focuses on the Cambrian-Ordovician boundary interval in western Inner Mongolia along the ancient northwest margin of the North China block in order to evaluate the early Paleozoic depositional history of this region. In this study, we present (1) a detailed sedimentary facies analysis of the Cambrian Series 3 Abuqiehai Formation and Middle Ordovician Sandaokan Formation, and (2) carbon isotope and detrital zircon geochronological data, which allow for regional and global stratigraphic and paleogeographic correlation, as well as refinement of the tectonic history of this poorly known part of the North China block.

GEOLOGIC SETTING

Our study area in the Zhuozishan Mountain area of western Inner Mongolia (Fig. 1), close to the Ordos highlands, exposes part of the western Ordos fold-and-thrust belt. This belt formed between the Early-Middle Jurassic and the Late Jurassic, possibly as an inland extension of deformation associated with subduction of a paleo–Pacific plate (Darby and Ritts, 2002). The main structure of Zhuozishan Mountain is basically a large basement-cored anticline (Darby and Ritts, 2002). Archean metamorphic basement and Proterozoic through Mesozoic sedimentary strata are exposed in the range. The North China block's metamorphic Archean–

Paleoproterozoic basement consists of Eastern and Western blocks, separated by the ca. 1.85 Ga Trans–North-China orogenic belt (Bian et al., 2001). This crystalline basement complex, which contains rocks that range in age from 3.85 to 1.6 Ga (Bian et al., 2001), underlies an ~107-m-thick Proterozoic succession.

Our study site is located in the northern part of the Helan aulacogen, which was connected to the western margin of the North China block. The Helan aulacogen, ~300 km in NNE trend, formed as a failed rift relative to the Qinling and Qilian rifts during the Mesoproterozoic, resulting in a thick (100–3000 m) terrestrial and shallow-marine sedimentary succession of conglomerate, quartz sandstone, and partly chertified dolomite strata intercalated with several layers of dolerite (Fig. 2; Sun and Liu, 1983). The succession nonconformably overlies Archean metamorphic rocks and generally thins toward the north. Regional uplift during the Neoproterozoic resulted in formation of an unconformity, and subsidence during the earliest Paleozoic led to deposition of Cambrian and Ordovician strata in shallow-marine to deep slope settings (Lin et al., 1991). The Helan aulacogen eventually closed in the Late Ordovician, and the subsequent uplift associated with a Caledonian orogenic event resulted in the absence of a Silurian through Mississippian record in this region and other parts of the North China block.

The Cambrian succession in the Zhuozishan area consists of a mixed siliciclastic and carbonate succession (Taosigou, Hulusitai, Zhangxia, and Abuqiehai Formations in ascending order), which disconformably overlies the Mesoproterozoic Wangquankou Formation. The Cambrian strata are underlain by an Ordovician succession (Sandaokan, Zhuozishan, Kelimoli, Wulalike, Lashenzhong, Gongwusu, and Sheshan Formations in ascending order), which is in turn disconformably overlain by the Pennsylvanian Yanghugou Formation (Fig. 2).

Chronostratigraphy		Formation	Major lithology
Pennsylvanian	Bashkirian	Yanghugou	Sandstone, coal, shale, limestone
Upper Ordovician	Katian	Sheshan	Turbidite sandstone, siltstone, shale, bioclastic grainstone
	Sandbian	Gongwusu	Greenish-gray mudstone, thin-bedded limestone, sandstone
		Lashenzhong	Turbidite sandstone, siltstone, shale
		Wulalike	Slump-debris flow deposits, black shale
Middle Ordovician	Darriwilian	Kelimoli	Graptolitic black shale, thin-bedded limestone, turbidite
		Zhuozishan	Bioturbated and bioclastic limestone, microbialites
		Sandaokan	Quartzose sandstone, bioclastic dolostone, limestone
Furongian	Fengshanian	Abuqiehai	Dolostone, carbonate conglomerate
	Changshanian		Thin-bedded limestone & dolostone, conglomerate
Cambrian Series 3	Kushanian		Bedded limestone, oolite, conglomerate
	Changhian	Zhangxia	Limestone-shale alternations, oolite, conglomerate
	Hsuchuangian	Hulusitai	Thin-bedded limestone, greenish-gray & purple shales
	Maochuangian	Taosigou	Sandstone, purple & greenish-gray shale, bedded limestone
Cambrian Series 2	Lungwangmiaoan		Sandstone, greenish-gray shale, dolostone
	Canglangpuan	Wudaotang	Dark gray dolostone, dolomitic limestone, limestone
		Suyukou	Phosphatic sandstone, glauconitic arkose sandstone
Ediacaran/Sinian		Zhengmuguan	Conglomerate, breccia, and gravelly sandstone; tillite
Mesoproterozoic	Jixian Sys.	Wangquankou	Minor sandstone, thick-bedded dolostone with stromatolite
	Changcheng Sys.	Huangqikou	Quartz sandstone, slate, and minor dolostone

Figure 2. Proterozoic to Paleozoic stratigraphy of western Inner Mongolia and Ningxia regions (i.e., Helanshan and Zhuozishan Mountains) of the North China block. Gray box shows stratigraphic range of the Subaiyingou section.

METHODS

Detailed sedimentological data were collected at the Subaiyingou section (SBG) along a well-exposed valley in Zhuozishan Mountain in western Inner Mongolia, China (Figs. 1, 3, and 4). Geochemical samples were collected for carbon-isotope chemostratigraphic analysis every ~25 cm throughout the sections. Samples were cut and microdrilled with a dental drill bit for powders, which were analyzed for carbon and oxygen isotopes at Washington University, St. Louis, Missouri. Powders were reacted for 4 h at 72 °C with an excess of 100% H_3PO_4 in He-flushed, sealed tubes. Evolved CO_2 was sampled with a Thermo Scientific Gas Bench II, and isotopic ratios were measured with a Thermo Scientific Delta V Plus mass spectrometer. Isotopic measurements were calibrated against standards NBS-19, NBS-20, and two in-house standards, with analytical errors of <0.1‰ (1σ) for $\delta^{13}C_{carb}$ and <0.2‰ (1σ) for $\delta^{18}O_{carb}$. All isotopic values are expressed in per mil (‰) notation relative to Vienna Peedee belemnite (VPDB).

Additionally, we collected a detrital zircon sample, SBGM-1, from the base of the Ordovician Sandaokan Formation at 19.72 m stratigraphic height in the Subaiyingou section. This sample was analyzed at the Research School of Earth Sciences, Australia National University, using a sensitive high-resolution ion microprobe (SHRIMP) with procedures given in Williams (1998, and references therein). Reflected and transmitted light photomicrographs, and cathodoluminescence (CL) scanning electron microscope (SEM) images were prepared for all zircon grains. The internal structures of the sectioned grains were imaged using CL and used

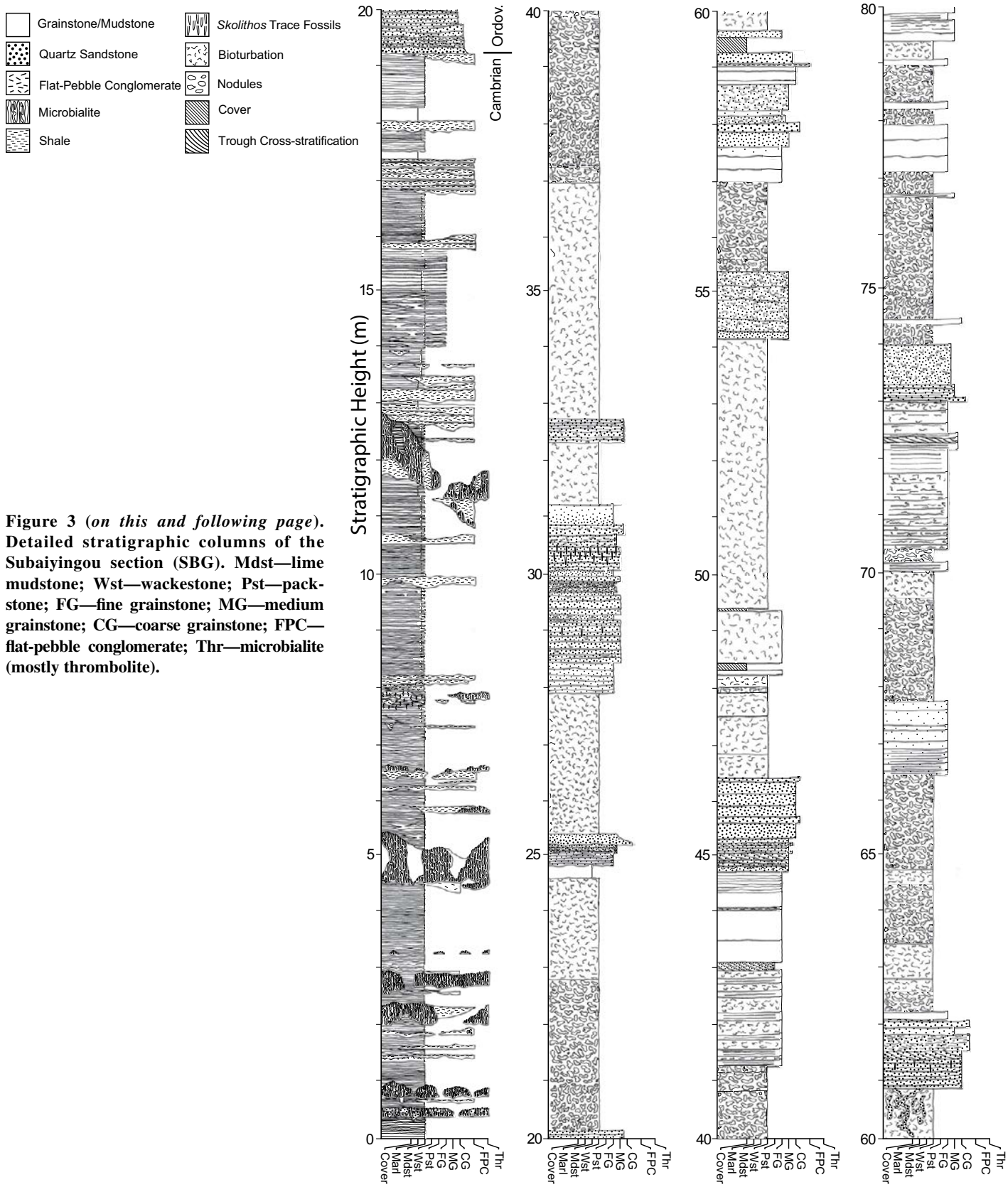

Figure 3 (*on this and following page*). Detailed stratigraphic columns of the Subaiyingou section (SBG). Mdst—lime mudstone; Wst—wackestone; Pst—packstone; FG—fine grainstone; MG—medium grainstone; CG—coarse grainstone; FPC—flat-pebble conglomerate; Thr—microbialite (mostly thrombolite).

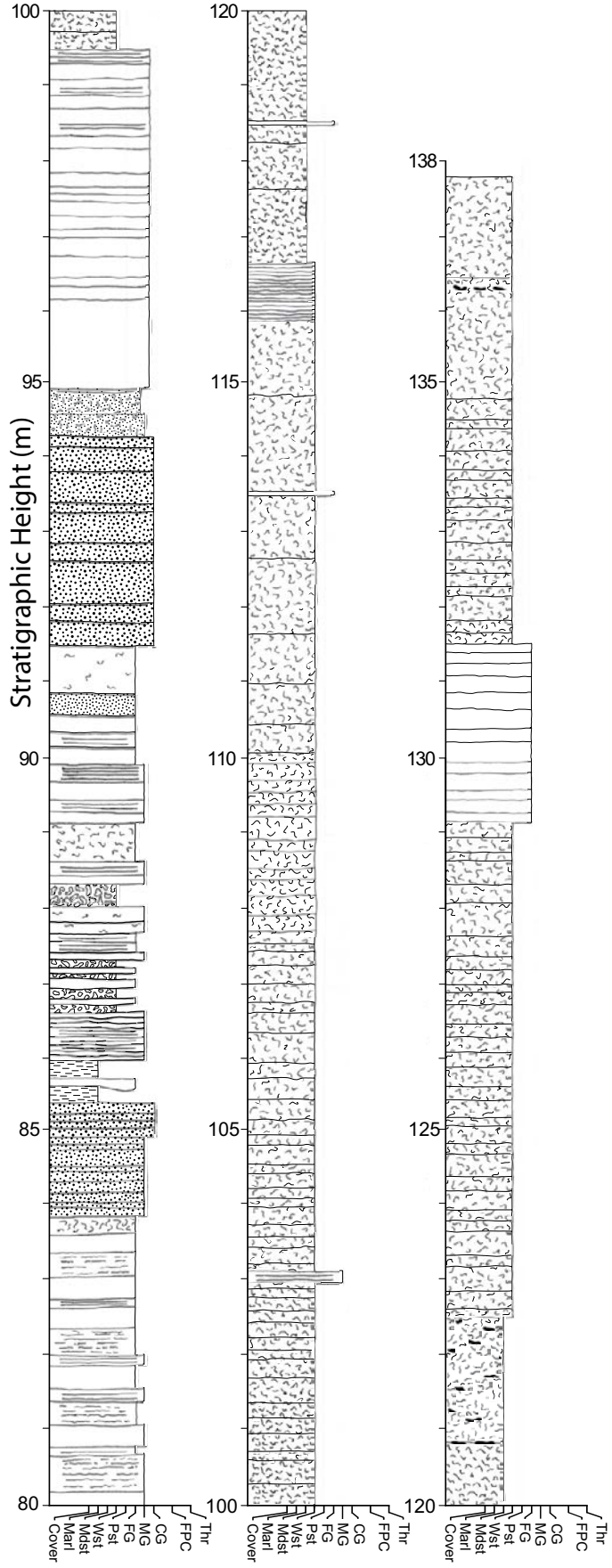

Figure 3 (*continued*).

to ensure that the ~20 μm SHRIMP spots were wholly within the youngest single age component (i.e., the rims) within the sectioned grains. The data for 70 grains were processed using the SQUID Excel macro (Ludwig, 2001). U/Pb ratios were normalized relative to a value of 0.0668 for the Temora reference zircon, equivalent to an age of 417 Ma (Black et al., 2003). Uncertainties given for individual analyses (ratios and ages) are at the 1σ level (see GSA Data Repository[1]). Correction for common Pb was made using the measured $^{204}Pb/^{206}Pb$ ratio in the normal manner, and the calculated radiogenic $^{207}Pb/^{206}Pb$ ages have been interpreted to constrain the individual spot dates. Two of the areas analyzed were significantly reversely discordant, and so the data for those grains are considered unreliable. Further, a number of other areas analyzed were discordant, and while in some cases this has resulted from radiogenic Pb loss at or near the present day, others clearly show older radiogenic Pb giving rise to the discordance. Analyses more than 10% discordant were not included in the relative probability plots.

Carbonate samples were processed for conodont microfossils using the buffered formic acid digestion method described by Jeppsson and Anehus (1995). Insoluble residues were processed using the cryogenic density separation technique described by Morrow and Webster (1989) with 2.85 SG LST (specific gravity lithium polytungstate) heavy liquid substituted for sodium polytungstate (SPT). Heavy fractions of the density separations were examined under a stereomicroscope, and conodont elements were picked from the residue, identified, and imaged using a Leo 1430VP SEM.

LITHOFACIES

Nine lithofacies are classified based mainly on lithology, grain size, and sedimentary structures, as well as texture, bed geometry, and fossil content (Fig. 3).

Interbedded Lime Mudstone and Marlstone Facies (L-M)

This facies consists of very thin to thin, 0.2–5-cm-thick, beds of lime mudstone and interbeds of dolomitic marlstone or calcareous shale (Fig. 5A). Lime mudstone layers are highly variable in character with tabular, undulatory, nodular, and irregular geometries, and both diffuse and distinct boundaries. The facies

[1]GSA Data Repository item 2015106, DR Item 1: detrital zircon geochronological data and associated plots; DR Item 2: carbon and oxygen isotopic data, is available at http://www.geosociety.org/pubs/ft2015.htm or by request to editing@geosociety.org.

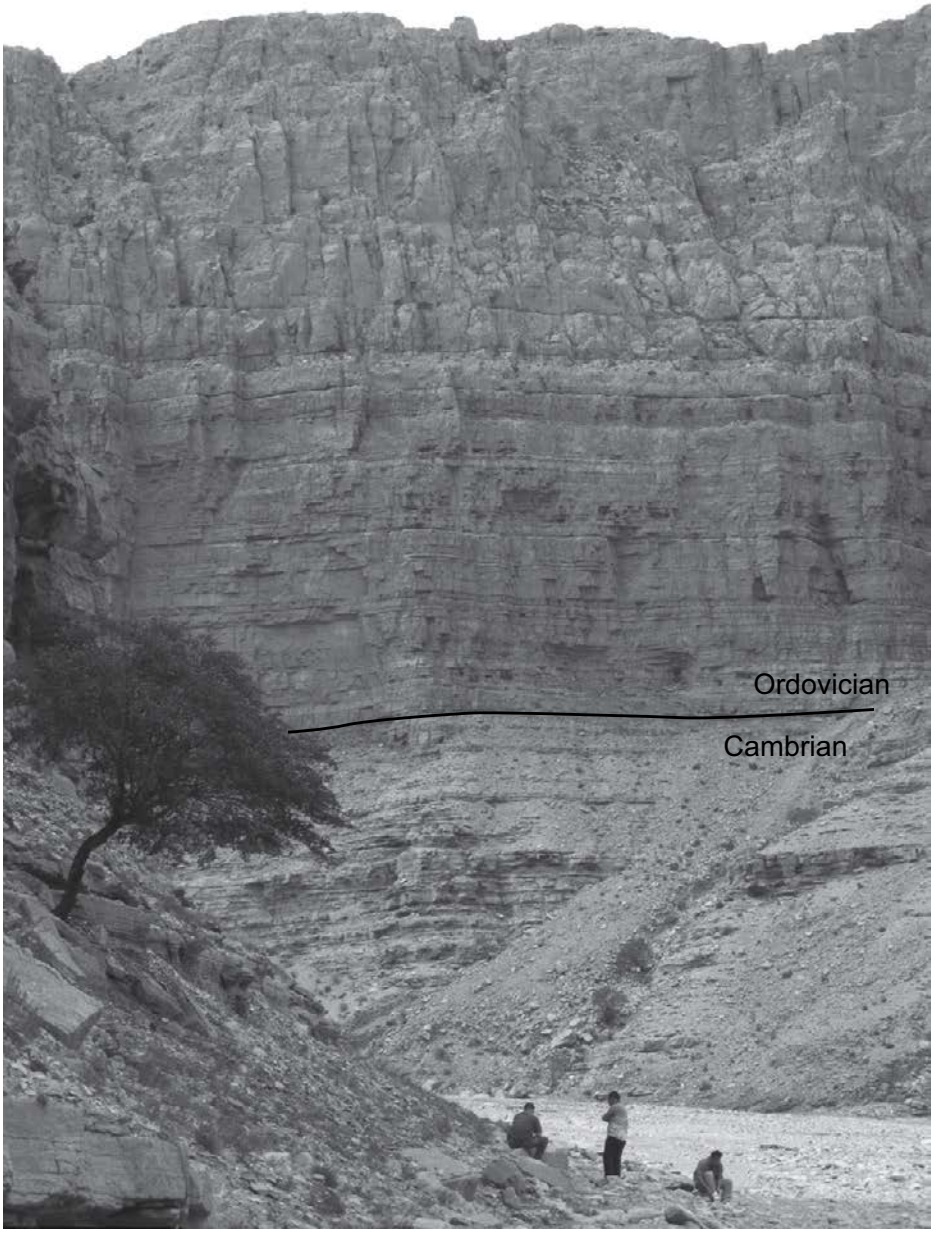

Figure 4. Full view of a wall of the Subaiyingou valley, showing well-exposed outcrop of the Cambrian and Ordovician strata. Cliff face is approximately 100 m tall.

varies from lime mudstone with thin marlstone or shale drapes, to marlstone with thin mudstone interbeds. Ball-and-pillow structures are locally present, and some beds are mildly bioturbated. This facies is commonly associated with flat-pebble conglomerate and microbialite facies (Figs. 5 and 6).

Interpretation

Exclusively clay-sized particles lacking lamination are indicative of deposition from suspension in a low-energy setting (Calvet and Tucker, 1988; Keller, 1997). The presence of both carbonate and siliciclastic material in varying proportions suggests that sediment was being supplied from both terrestrial and in situ marine sources, with varying influence from one or both sources. The presence of bioturbation most likely indicates a marine depositional setting, and the local and sporadic stratigraphic distribution suggests that environmental conditions were unsuitable for extensive colonization and generally inhospitable to marine organisms. The nodular weathering pattern and pinch-and-swell structures in many beds of this facies are likely diagenetic features (Chen et al., 2009, 2010).

Flat-Pebble Limestone Conglomerate Facies (LCfp)

Flat-pebble conglomerate consists of oligomicitic to polymictic limestone clasts and bioclastic grainstone matrix (Figs. 5B–5E). Beds of this facies exhibit both clast-supported and matrix-supported textures. Clasts are mostly flat lying and locally imbricated (Fig. 5B); in a few cases, they are vertically oriented. Flat-pebble conglomerate beds are tabular to lenticular and range from 4 to 47 cm thick. Amalgamated conglomerate beds range up to 48 cm thick. Flat-pebble conglomerate beds are commonly intercalated within thin-bedded limestone beds, and in cases comprise small gutter casts (Fig. 5C) or mounds (Fig. 5D), which range from 4 cm thick and 17 cm wide to 9 cm thick and 33 cm wide. Flat-pebble conglomerate is also often present around and between microbialite mounds (Fig. 5E). Most flat-pebble conglomerate beds show sharp, irregular, and locally channelized bases. Normal grading is rarely present in the flat-pebble conglomerate.

Interpretation

Flat-pebble conglomerate is thought to result from storms in shallow-marine environments (Mount and Kidder, 1993; Myrow et al., 2004, 2012; Chen, 2014). Clasts produced by erosion and rip-up of early-cemented carbonate sediment during storms were transported by storm-generated waves and associated currents, and in instances by gravity forces (Myrow et al., 2004, 2012; Chen, 2014). Mostly flat-lying clasts indicate constant reworking of waves, whereas imbricated clasts indicate reworking by currents. The rare examples with vertical imbrication are attributed to clast interactions under storm waves. The clasts were deposited along with winnowed bioclastic grains, which is typical of ancient flat-pebble conglomerate facies (Myrow et al., 2004). The lack of evidence for subaerial exposure (e.g., mud cracks) in associated facies suggests deposition in subtidal regions. The presence of flat-pebbles in gutter casts suggests initial erosion by powerful bottom currents (Myrow, 1992) and subsequent filling with intraclasts eroded during the storm event.

Maceriate Microbialite Facies (Mm)

The microbialite facies is characterized by digitate or maceriate (maze-like) vaguely stromatolitic and thrombolitic structures (Figs. 6A and 6B), and this facies is composed of microstromatolites with associated patches of sponge spicules (Figs. 6C and 6D). They commonly show mounded or highly irregular morphologies and are laterally adjacent to detrital carbonate

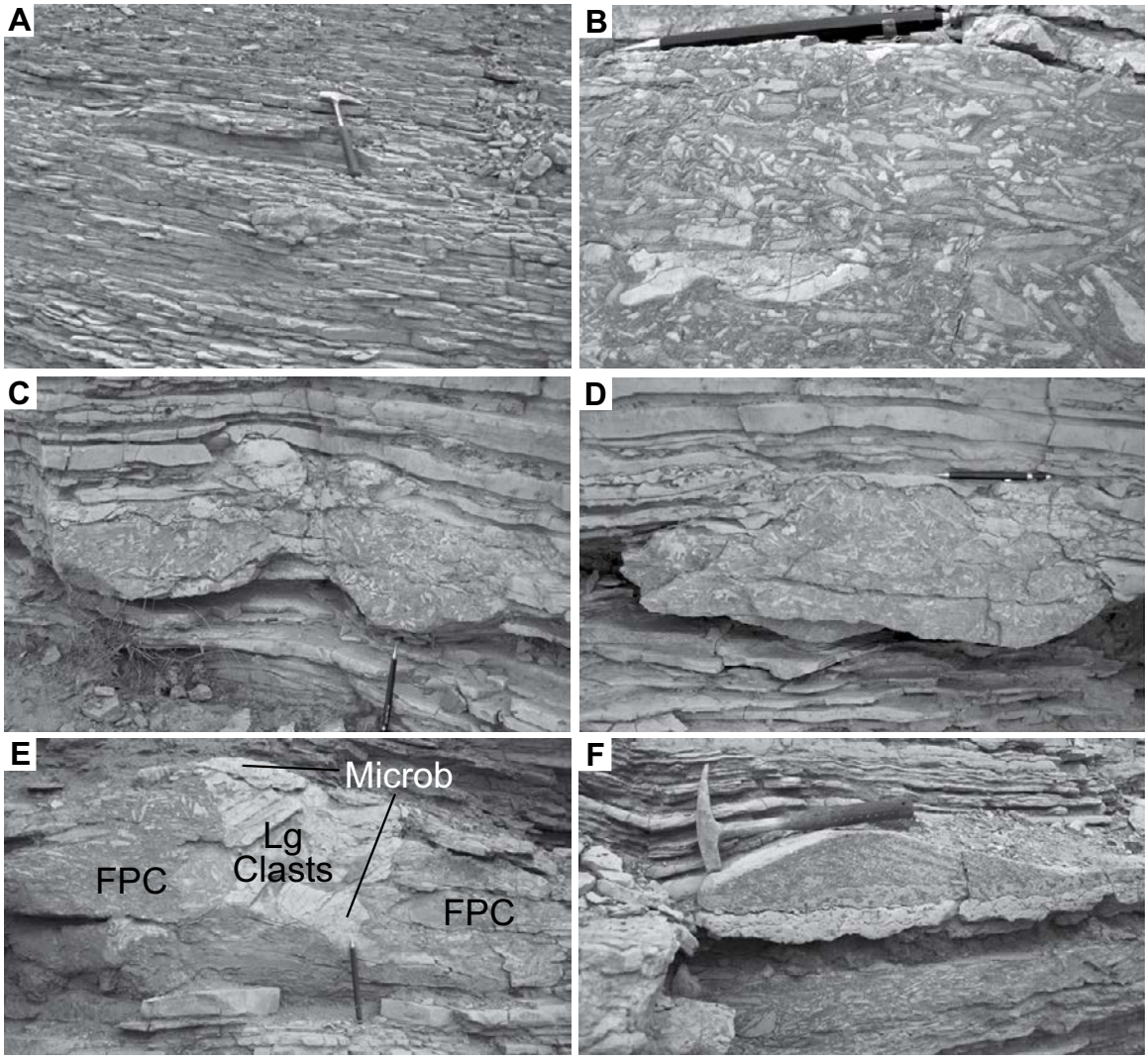

Figure 5. Representative photos of lithofacies. (A) Thinly interbedded lime mudstone and marlstone facies. Note lens of flat-pebble conglomerate below hammer (scale). (B) Close-up of fabric of flat-pebble conglomerate facies showing abundant brown grainstone matrix and subhorizontal orientations of lime mudstone clasts. (C) Gutter casts of flat-pebble conglomerate within mudstone and marl facies. (D) Mounded lens of flat-pebble conglomerate. (E) Mounded mass of flat-pebble conglomerate (FPC), large clasts of rotated, relatively intact-bedded lime mudstone, and masses of microbialite. (F) Symmetrical starved ripple of coarse grainstone. Most cross-laminae dip to right, but some dip to left on left flank. Hammer is 30 cm long, and pencil is 14 cm long, for scale.

sedimentary deposits. Most microbialite mounds are 15–40 cm thick, although some range in size up to 1.2 m thick and >1 m wide. In several places, the microbialites either form complexes with, or occur within, beds of intraclast conglomerate. Between 4.53 and 5.43 m in the Subaiyingou section, microbialite mounds form a thick complex with dark-gray/brown, fine to medium grainstone. In general, the microbialite weathers brown to orange, and the intermicrobialite fill is white or gray. Between 10.81 and 11.83 m in the Subaiyingou section, thick microbialite mounds rest on a conspicuous erosional surface that gradually cuts out ~94 cm of underlying strata (Fig. 6E). These microbialite mounds are surrounded by flat-pebble conglomerate at the base, and by ribbon mudstone and calcareous shale at the top.

Interpretation

These microbialites resemble the recently studied maceriate microbialites from the eastern North China block (Shandong region) and Laurentia (Shapiro and Awramik, 2006; Lee et al., 2010, 2012, 2014; Chen et al., 2014; Chen and Lee, 2014). The well-preserved microbialite from the Shandong region is composed of abundant sponge spicules and microbial components, for which it is also called "sponge-microbial reef" (Lee et al., 2014; Chen et al., 2014). The presence of patches of sponge spicules indicates that the microbialites from the Subaiyingou section are similar to those in Shandong province, with respect to their micro- and macrostructures. The fine-grained texture of microbialites and associated limestone-shale alternations are indicative of relatively low-energy settings during growth of microbialites. Brown to orange color of the microbialite is due to selective dolomitization. Overlying and lateral deposits of flat-pebble conglomerate, irregular morphology of microbialite buildups by erosion, and irregular bases with locally high relief are collectively suggestive of intermittent high-energy conditions.

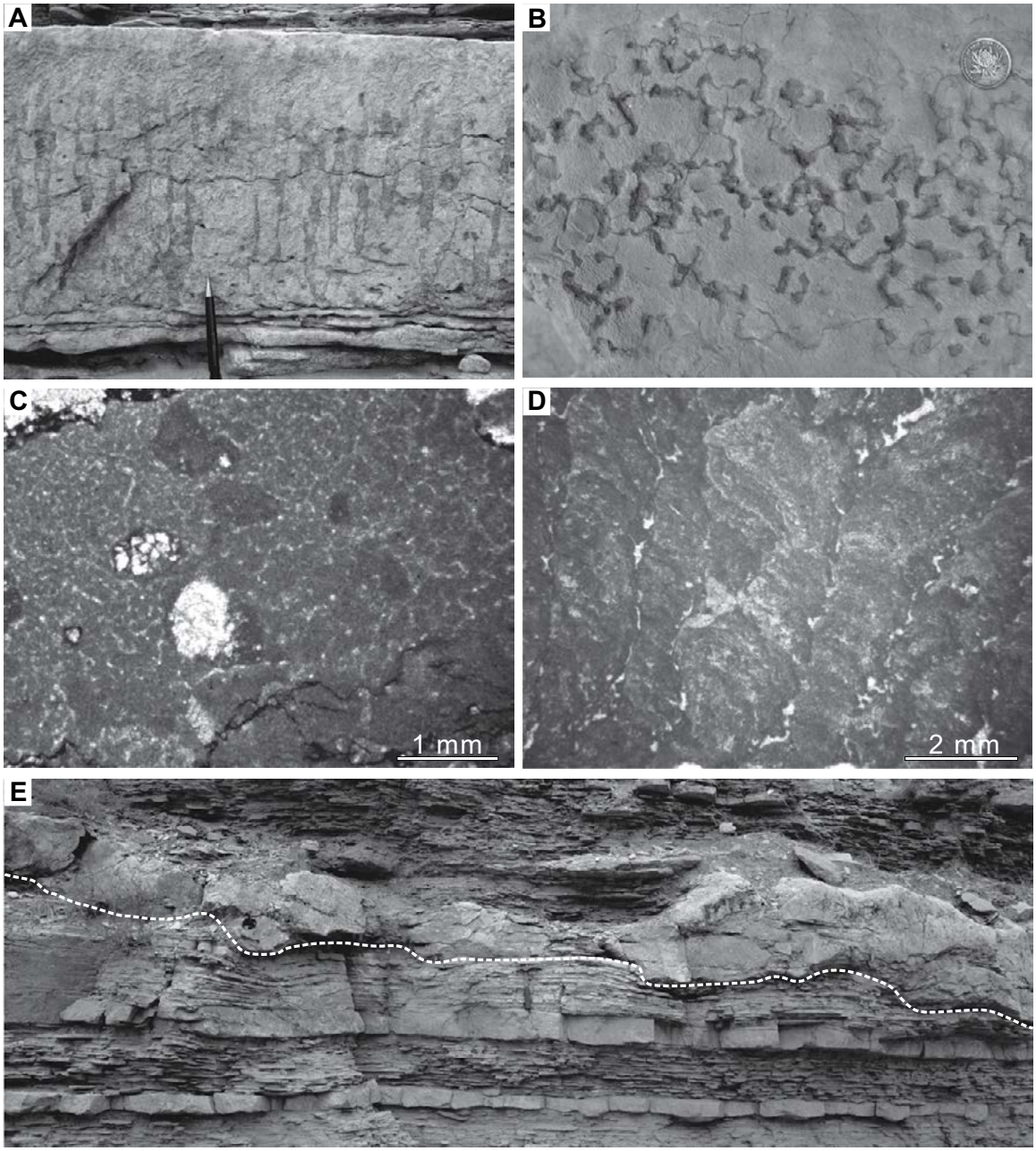

Figure 6. Maceriate microbialite facies. (A) Vertical section of a maceriate microbialite, showing digitate, branching structures (i.e., maceriate structures of Shapiro and Awramik, 2006). (B) Bedding plane of a maceriate microbialite, showing rambling, maze-like structures. Coin is 25 mm in diameter. (C) Patch of sponge spicules in a maceriate microbialite. (D) Microstromatolite in a maceriate microbialite. (E) A maceriate, thrombolitic microbialite and flat-pebble and grainstone complex, downcutting the underlying strata via an irregular surface. Hammer is 28 cm long, and pencil is ~12.5 cm long, for scale.

Fine to Medium Sandy Grainstone Facies (Gfm)

This facies is composed of massive, bioturbated, and parallel-laminated, well-sorted, fine and medium grainstone and dolograinstone. The grainstone contains up to 40% grains of quartz sand. Bed thickness ranges from 1 to 93 cm, with an average of ~25 cm. Burrows are present in some beds. Beds are generally tabular and have uniform thickness. From 24.84 to 25.07 m, there are amalgamated, hummocky cross-stratified, thin sandy grainstone beds. The basal bed in this interval has a locally scoured base. One set of beds between 86–86.64 m is poorly sorted, with grains ranging from fine to coarse sand. Also, one set of beds between 72.19 and 72.48 m exhibits ripple-scale cross-stratification and parallel lamination.

Interpretation

The presence of ripple cross-lamination, parallel lamination, and hummocky cross-stratification indicates traction transport and

deposition under the influence of unidirectional and oscillatory flows of variable intensity. Hummocky cross-stratification in particular indicates deposition from powerful storm-generated waves (Myrow and Southard, 1991, 1996; Dumas et al., 2005). Fully bioturbated beds suggest periods of lower energy and colonization by infaunal organisms in a shallow-marine depositional environment.

Coarse Grainstone Facies (CG)

This facies consists of beds up to 20 cm thick of massive and laminated, gray to dark-gray, coarse bioclastic grainstone. Bedding is generally tabular, although some beds are lenticular. Coarse grainstone is commonly intercalated with the L-M facies and sometimes forms an irregular complex with thrombolitic microbialite mounds. It also forms cross-laminated form sets of generally symmetrical ripples up to 8 cm in height (Fig. 5F). The cross-lamination tends to dip in one direction, even in ripples with nearly symmetrical profiles (Fig. 5F).

Interpretation

The coarse grain size of this facies represents deposition of winnowed sediment under high-energy flows. It is possible that these deposits were either storm generated or reworked by storms, based on the presence of symmetrical ripples, although the grain size is too coarse to exhibit wave-diagnostic hummocky cross-stratification. The massive texture of the facies may reflect diagenetic alteration that masks macroscopic lamination.

Sandstone Facies (SS)

This facies consists of white, tan, and brown, very fine to very coarse quartz sandstone (Fig. 7). Some units are massive or bioturbated (Figs. 7A and 7B), whereas others contain parallel lamination and trough cross-stratification (Fig. 7C). Bed thicknesses range from 3 to 32 cm, and many are part of amalgamated bed sets that range from 0.30 to 2.97 m thick. The sandstone in most beds is relatively well sorted, but some beds are poorly sorted with grain sizes ranging either from fine to coarse or medium to very coarse sand. A few beds show normal grading and, in cases, contain granules to fine pebbles at their bases. Trough cross-stratified sets are 3–12 cm thick. Several beds contain small (1–2 mm thick) floating intraclasts of carbonate mudstone. The sandstone grains are generally subrounded. Many sandstone beds contain burrows, including, in some cases, *Skolithos* (Fig. 7A).

Interpretation

The presence of trough cross-bedding reflects deposition by migration of three-dimensional (3-D) dunes by unidirectional currents, whereas parallel lamination indicates deposition from upper plane bed conditions. The high variability in grain size and degree of sorting indicates highly variable energy levels and constancy of energy. The close stratigraphic association with marine carbonate (e.g., bioturbated wackestone and grainstone), and the presence of bioturbation and *Skolithos* trace fossils in some beds are consistent with this facies having been deposited in a shallow-marine environment, most likely in a shoreline setting.

Calcareous Sandstone Facies (SSc)

This facies consists of poorly sorted to very poorly sorted, bioturbated, medium or fine/medium quartz sandstone with 20%–50% carbonate grains. Bed thicknesses range from 11 cm to 69 cm. Two beds, at 54.23 and 61.86 m, lack bioturbation. One bed, at 30.88 m in the Subaiyingou section, grades upward from 80% quartz sandstone at its base to fine grainstone with ~5% quartz grains at its top.

Interpretation

The finer grain size and better sorting of this facies, relative to the sandstone facies (SS), reflect deposition in a lower-energy environment, although likely in a nearshore to shoreline setting based on the abundance of quartz grains and the bioturbation. These features would be consistent with a lower shoreface setting where terrestrial-derived quartz sand mixed with offshore carbonate in the transition zone with the offshore. Compete bioturbation is common in lower shoreface to offshore transition zones, reflecting a transition from laminated sediment higher on the shoreface, which is frequently reworked by marine currents and waves, to sediment that is less frequently mobilized.

Bioturbated Wackestone Facies (Wb)

This facies consists of moderately to severely bioturbated lime mudstone to wackestone (ichnofabric index 3 and 4 of Droser and Bottjer, 1986), with mottled texture due in part to selective dolomitization (Fig. 8A). The wackestone is composed dominantly of lime mud and various fossil fragments (trilobites, bivalves, and brachiopods; Fig. 8B). Some disarticulated brachiopods are present in bioturbated wackestone. Bed thicknesses range from ~8 cm to 4.82 m. Some beds exhibit a nodular dolomitization pattern, with 30% to 100% of the facies dolowackestone, whereas other beds exhibit no dolomitization at all. The color of these beds is chocolate brown on weathered surfaces, whereas fresh surfaces of the nondolomitized limestone are light blue. An ~90-cm-deep paleokarst is present in bioturbated wackestone at 60.91 m in the Subaiyingou section and is overlain by a 1.28-m-thick unit of quartz sandstone (Fig. 9). The paleokarst consists of a network of irregular branching sand-filled cavities that cut the wackestone host rock. They have highly irregular, sharp, and scalloped margins and contain a fill of quartz grains ranging in size from medium to coarse sand up to granules (Fig. 9). Several 3–7-cm-thick coarse sandstone beds that overlie the paleokarst (described in the following) are deformed, with downwarping of the sandstone laminae into the underlying depression in the wackestone (Fig. 9C).

Interpretation

The extensive and pervasive bioturbation is suggestive of shallow subtidal environments with relatively low sedimentation rate (Rubin and Friedman, 1977; Overstreet et al., 2003). The abundance of lime mudstone is indicative of low-energy environments protected from waves or currents (e.g., lagoon or offshore; Sanders and Hofling, 2000). The common presence of fossil fragments of typical marine fauna suggests that deposition took place in shallow subtidal environments with normal salinity (Heckel, 1972). The presence of disarticulated brachiopod fossils suggests minor transport of larger fossils. Based on its association with quartz sandstone facies of likely shoreline origin, we interpret this facies as having been deposited below fair-weather wave base in a proximal offshore region. The presence of paleokarst in the bioturbated wackestone indicates that it was subaerially exposed and chemically weathered after cementation. Deformation of sandstone above the paleokarst suggests partial collapse into the karst cavities after its deposition. The paleokarst developed at one stratigraphic level after significant lowering of base level at that time to expose previously deposited subtidal marine strata.

Shale Facies (Sh)

This facies consists of greenish-gray and dark-gray, silty and marly shale. Bed thickness ranges from 1 to 24 cm.

Interpretation

Deposition of clay- and silt-sized particles requires deposition from suspension in a very low-energy setting, most likely below fair-weather wave base (Chen et al., 2011). The dominantly siliciclastic facies suggests that it may have formed during times of high terrestrial input and/or depression of carbonate production (Chen et al., 2011; Myrow et al., 2012). The

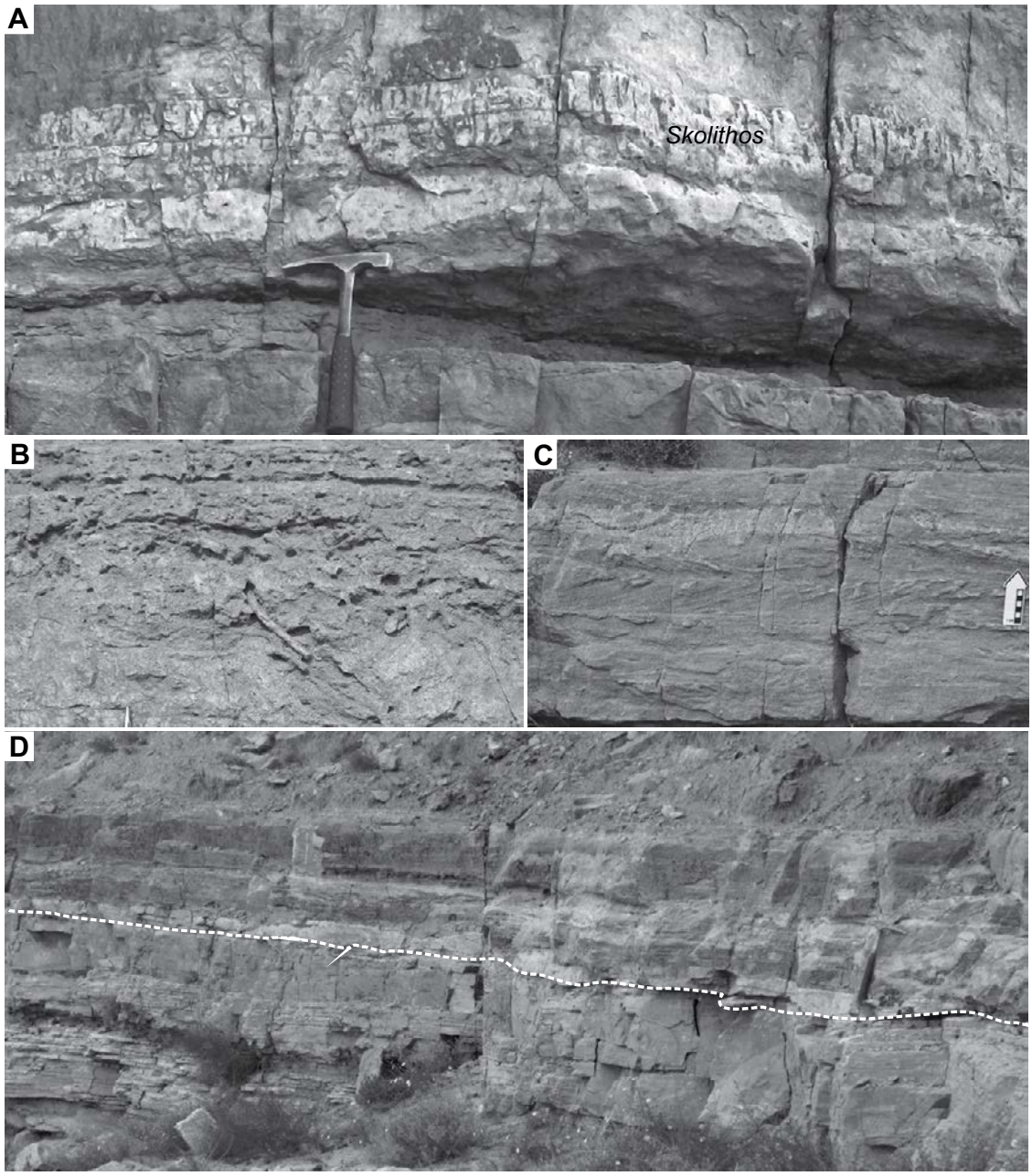

Figure 7. Sandstone facies in Ordovician strata. (A) White and brown weathering sandstone with bed containing abundant *Skolithos* trace fossils. Hammer is 28 cm long. (B) Bioturbated sandstone. Pencil tip in the lower left for scale. (C) Trough cross-stratified sandstone. Scale bar is in centimeters. (D) Contact between orange-weathering uppermost Cambrian dolostone and Ordovician sandstone and bioturbated mudstone. Hammer is 30 cm long.

dark color of shale reflects high organic carbon content and is indicative of relatively reducing conditions (Myrow, 1990).

FACIES ASSOCIATIONS

Based on the occurrence of facies and stratigraphic arrangement, the 10 lithofacies are generally grouped into two facies associations, i.e., Abuqiehai and Sandaokan Formation facies associations. The Abuqiehai facies association consists dominantly of lime mudstone and marlstone alternation (L-M), flat-pebble limestone conglomerate (LCfp), and maceriate microbialite (Mm) lithofacies, whereas the Sandaokan facies association dominantly contains bioturbated wackestone (Wb), fine to medium grainstone facies (Gfm), shale facies (Sh), coarse grainstone facies (CG), sandstone facies (SS), and calcareous sandstone facies (SSc).

Facies Association Interpretations: Cambrian Abuqiehai Formation

The Abuqiehai strata exhibit many features typical of storm-dominated offshore settings, including hummocky cross-stratification, flat-pebble conglomerate, and gutter casts. The interbedding of various carbonate lithofacies and shale, combined with a low paleolatitude (Huang et al., 2000), indicate that the setting was a warm,

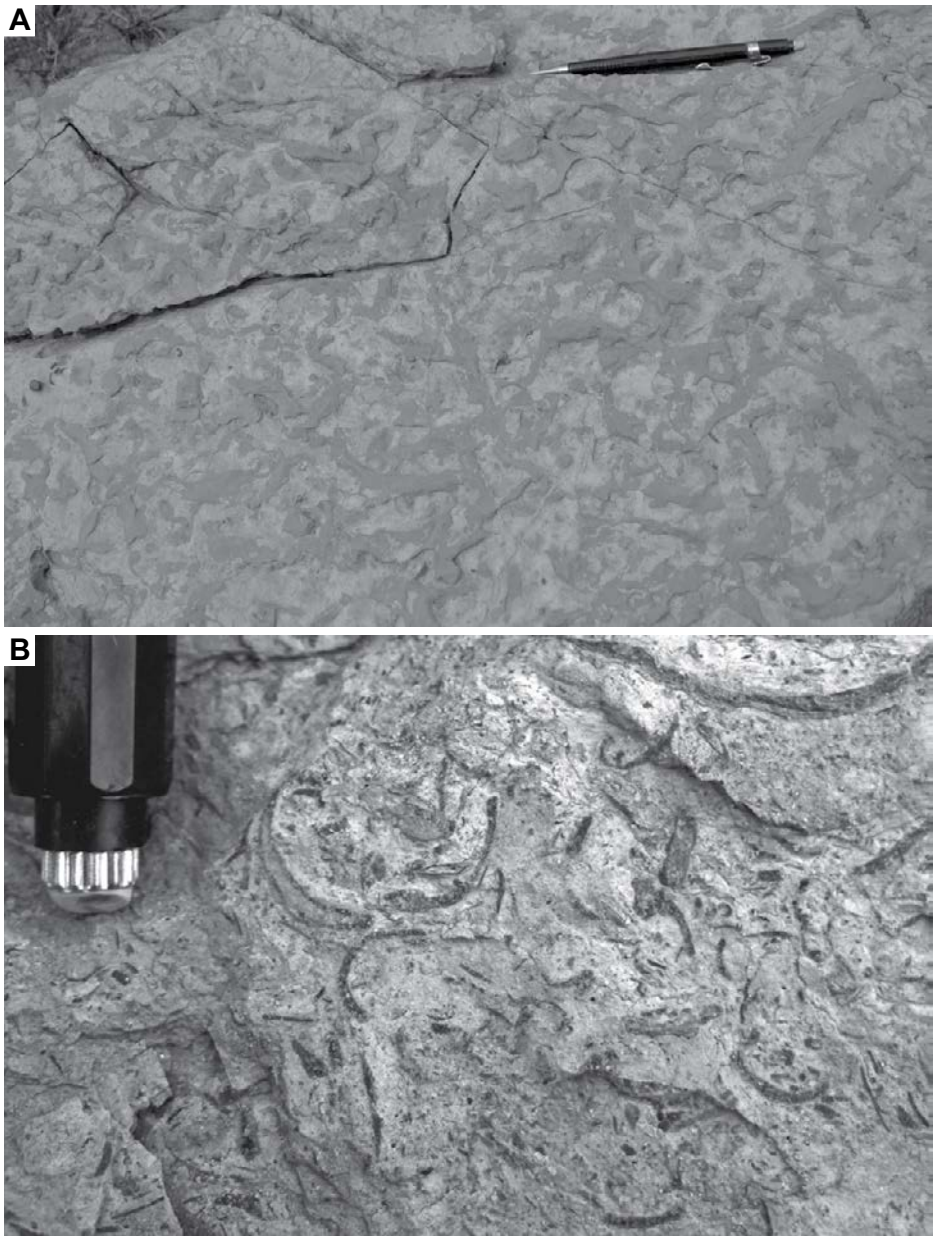

Figure 8. Bioturbated wackestone facies. (A) Dolomite-replaced burrows within lime wackestone. (B) Close-up showing dispersed bioclasts within the mudstone matrix. Pencil is 14 cm long, for scale.

shallow-water setting in which the production of carbonate near the shoreline was interrupted episodically by fine-grained terrigenous input from the Ordos highlands. Thus, a proximal siliciclastic mud-dominated detrital belt formed, with carbonate production likely distal to it.

The facies are identical to those of the Cambrian inner detrital belt of Laurentia, which was situated between a cratonic hinterland and a more distal carbonate belt (Lochman-Balk, 1971; Li and Droser, 1997; Myrow et al., 2003, 2004, 2012; Runkel et al., 2012). In this setting, there was interplay between in situ carbonate sediment production and temporal changes in fine-grained detrital mud input linked to unsteady runoff and sediment transport (Myrow et al., 2012). These facies are also similar to those interpreted as storm-influenced middle-outer ramp settings below fair-weather wave base where reworked carbonate sediment and suspended siliciclastic fines were deposited together (e.g., Markello and Read, 1981; Burchette and Wright, 1992; Meng et al., 1997; Kwon et al., 2006).

In this study, the presence of such features as carbonate beds with micro-hummocky cross-stratification and flat-pebble conglomerate suggests episodic storm-generated transport of carbonate grains into an environment characterized by accumulation of terrestrial mud. Changes in the overall percentages of carbonate and siliciclastic strata in such mixed lithofacies have been commonly linked to relative sea-level changes. In some ancient settings, such as the interface of a carbonate ramp and a deeper-water setting, rising sea level led to retreat of the carbonate belt and reduced input of carbonate sediment, and thus encroachment of a mud belt over the carbonate platform (Markello and Read, 1981; Calvet and Tucker, 1988; Chen et al., 2011, 2012). Myrow et al. (2012) suggested that in inner detrital belt settings, the reverse may be the case, namely, that during lowstands, rejuvenated fluvial systems may have increased mud input and stifled carbonate production, whereas during transgression, landward migration of shorelines may have led to alluviation, reduced sediment input, and increased carbonate production and deposition. It is possible that the flat-pebble conglomerate and thrombolite complexes of the Cambrian Abuqiehai Formation of this study formed during maximum flooding intervals when the seawater was less turbid and probably warmer (cf. Myrow et al., 2012) than at other times. On the other hand, such intervals could also reflect long-term changes in storm intensity and associated sediment transport. In either case, the association of thrombolites resting on flat-pebble conglomerate beds reflects preferential colonization of microbes on hard substrates (e.g., Myrow et al., 2012).

Finally, the general paucity of shale, relative to marl, suggests an overall low amount of siliciclastic mud input, which is consistent with the fact that only a very small part of the North China block was above sea level during the Cambrian to act as a source of fine-grained siliciclastic sediment (e.g., Meng et al., 1997; Feng et al., 2002).

Facies Association Interpretations: Ordovician Sandaokan Formation

The basal Ordovician deposits of this study, the Middle Ordovician Sandaokan Formation, directly, unconformably overlie uppermost Cambrian Series 3 strata. The Sandaokan Formation consists dominantly of carbonate lithofacies and widely spaced quartzose sandstone units. The nature of the sandstone lithofacies and the presence of marine trace fossils, in combination with sandstone-filled paleokarst in bioturbated wackestone at 60.91 m in the Subaiyingou section, clearly indicate shoreline deposition.

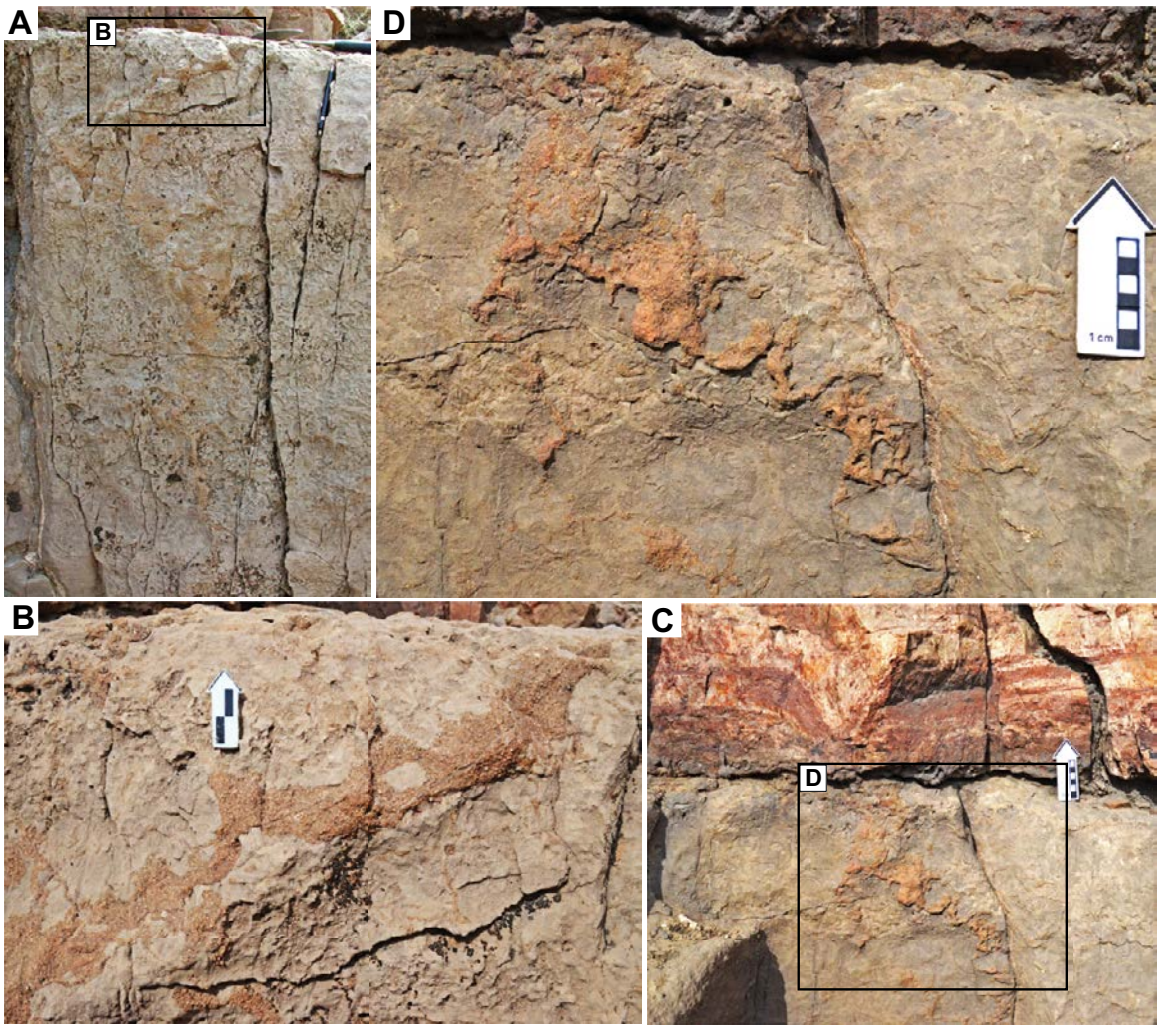

Figure 9. Examples of the paleokarst fills between meters 60 and 61 of the Subaiyingou section. (A) Bioturbated wackestone with sandstone-filled paleokarst. (B) Close-up of a sandstone-filled paleokarst in wackestone. (C) Bioturbated wackestone bed with sandstone-filled paleokarst, overlain by partly deformed sandstone. (D) Close-up of sandstone-filled paleokarst in wackestone. Pencil is 14 cm, and scale bar is in centimeters.

The close association of shoreline quartzose sandstone deposits and marine carbonate facies (mostly bioturbated wackestone) indicates that the general depositional environment during the Ordovician was the proximal part of a carbonate shelf. The relatively sharp contacts between the sandstone facies and overlying bioturbated wackestone facies reflect a sharp paleoenvironmental transition from shoreline to a low-energy carbonate shelf setting that was episodically influenced by transport and deposition of carbonate sand by storm waves. Alternation of sandstone and wackestone thus reflects relative sea-level changes. A few beds of calcareous sandstone and fine- to medium-grained sandy grainstone indicate mixing of carbonate and siliciclastic sediment at times.

On a larger scale, the upward stratigraphic decrease in abundance and increased spacing of quartzose sandstone beds likely reflect transgression and retrogradational stacking of parasequences, for which lowstands are represented by the sandstone facies. The eventual stratigraphic loss of sandstone in the lower Sandaokan Formation reflects a transgressive landward shift of shoreline environments. Although a full sequence stratigraphic analysis of this formation is beyond the scope of this study, the lower Sandaokan Formation records a transgressive systems tract with a series of relatively high-order parasequences.

DETRITAL ZIRCON GEOCHRONOLOGY

The spectrum for sample SBGM-1 from the Ordovician strata of the Subaiyingou section contains grain ages from ca. 1400 Ma to ca. 3150 Ma (Fig. 10). It contains two significant age populations: ca. 1700–2000 Ma and ca. 2400–2550 Ma, including large peaks at ca. 1820 Ma and ca. 2520 Ma. The concordia diagram indicates some radiogenic Pb loss has occurred in a few of the areas analyzed (DR Item 1 [see footnote 1]). For the prominent Archean grouping, this appears to have occurred along a discordia toward a lower intercept at ca. 550 Ma. The upper intercept is at ca. 2520 Ma, while the age peak for the $^{207}Pb/^{206}Pb$ ages is at ca. 2515 Ma. For the Paleoproterozoic grouping, some of the areas appear to have lost radiogenic Pb in the Triassic, although both these trends may be mixing lines, and so the lower intercepts are of doubtful geological significance. The dominant Paleoproterozoic age grouping has an upper intercept at ca. 1860 Ma, while the age peak for the $^{207}Pb/^{206}Pb$ ages is at ca. 1815 Ma.

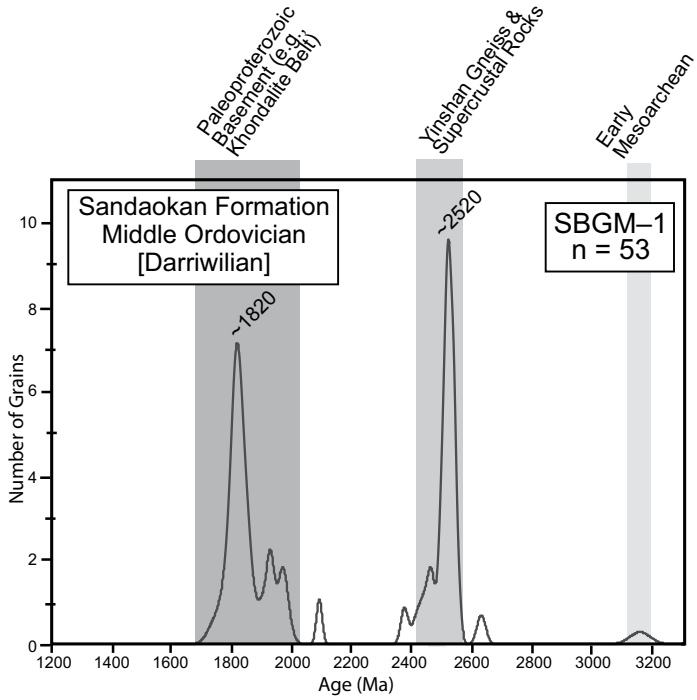

Figure 10. Detrital zircon spectrum for sample SBGM-1, from the Middle Ordovician (Darriwilian) Sandaokan Formation. The relative age probability diagrams show ages and uncertainty (plotted as a normal distribution about the age).

Although there is a general paucity of geochronological data on basement rocks in this area of Inner Mongolia (Darby and Gehrels, 2006), there is good agreement between the SBGM-1 spectrum and the ages of some crystalline basement rocks of the western margin of the North China block. For instance, ca. 2.5 Ga trondhjemite-tonalite-granodiorite (TTG) gneisses and supracrustal rocks exist in the Yinshan part of the western block, and zircon ages from the Khondalite belt range from 2.3 to 1.85 Ga (Darby and Gehrels, 2006). This suggests that sediment was likely being supplied to the Subaiyingou area primarily from exposed parts of the North China block, and not other crustal blocks. The Subaiyingou section is proximal to the ancient western North China block Ordos highlands of the Late Cambrian to Middle Ordovician, and thus the nearshore sandstone SBGM-1 sample may exclusively reflect local transport from those highlands, even if there were a tectonic connection between the North China block and another landmass at the time. Darby and Gehrels (2006) noted that Neoproterozoic and Cambrian strata in this area had slightly different detrital zircon age signatures from those of an Ordovician sample, and they speculated that there was a change in source between the Cambrian and Ordovician.

Various early Paleozoic paleogeographic reconstructions have been produced for the North China block, most of which involve a Cambrian connection with Gondwana. Paleomagnetic investigations indicate that the latitude of the North China block during the Early Cambrian was ~17°S (Huang et al., 2000), which is consistent with the predominance of warm shallow-water carbonate lithofacies in the North China block's Cambrian sedimentary units. Burrett and Richardson (1980) presented the North China block as an outboard terrane at a low northern latitude, proximal to Australia, during the Early Cambrian. Huang et al. (2000) depicted it as attached to the paleo-Pacific side of Antarctica during the Cambrian, until detachment in the Early Ordovician and subsequent migration to reside outboard of Siberia. Li and Powell (2001) showed the North China block as outboard of, but proximal to, the paleo–Pacific margin of Gondwana throughout the Cambrian, and potentially into the Ordovician. Recently, McKenzie et al. (2011) placed the North China block connected to, and sharing a detrital belt with, the northern margin of India during the Cambrian.

McKenzie et al. (2011) presented detrital zircon spectra of two samples taken from Cambrian strata of the North China block. A sample taken from the eastern North China block margin contains grains with peaks similar to those of SBGM-1 (ca. 1815 Ma and ca. 2515 Ma), as well as a range of younger grains up to ca. 500 Ma. A North China block southern margin sample exhibits a spectral pattern that lacks ca. 1600 Ma and ca. 2500 Ma peaks but matches Cambrian–Ordovician spectra from northern India, again with a wide range of grain ages up to ca. 500 Ma. McKenzie et al. (2011) interpreted their spectra, in combination with paleobiogeographical relationships between the North China block and India, as representing a tectonic connection and a shared detrital belt with sediment input from both masses. The abundance of ca. 500 Ma zircon grains in north Indian detrital samples, as well as a period of metamorphism in northern India (Gehrels et al., 2003) provide some support for the idea of a shared Cambrian tectonic event between India and the North China block.

Our spectra from the Subaiyingou section, which suggest local derivation from the Ordos highlands, stand in striking contrast to the existing Cambrian and Ordovician spectra from the North China block and from other sites in East Gondwana, including Antarctica (Goodge et al., 2004), Australia (Fergusson et al., 2007), and northern India (Myrow et al., 2010). Specifically, there is (1) a lack of grains younger than 1385 Ma, including a globally ubiquitous ca. 500 Ma peak associated with widespread granitic pluton emplacement due to the final assembly of Gondwana (e.g., Veevers, 2004; Blakey, 2008; Meert and Lieberman, 2008), and (2) abundant grains between ca. 1700 Ma and ca. 2000 Ma, which are relatively rare to absent in the spectra of Ordovician strata from Pakistan and India (Myrow et al., 2010). This difference does not support, but also does not rule out, a possible tectonic connection between the North China block and one or more of these continents during the early Paleozoic.

CARBON ISOTOPE CHEMOSTRATIGRAPHY

Carbon isotope ($\delta^{13}C$) data (DR Item 2 [see footnote 1]) for the Cambrian Abuqiehai Formation of the Subaiyingou section are characterized by short-period oscillations that are generally between 0.2‰ and 0.6‰ (Fig. 11). There is a –1.3‰ jump at 19.24 m across the unconformity at the Cambrian-Ordovician boundary (cf. Saltzman et al., 1998; Chen et al., 2011). Values in the overlying Ordovician strata are initially ~–1.5‰, drift slightly more negative to ~–2‰, and then drift positively over the next 70+ m to ~–0.6‰. The falling limb of this excursion shows a general shift of ~1.5‰ (Fig. 11). Superimposed over these trends, there is higher-frequency

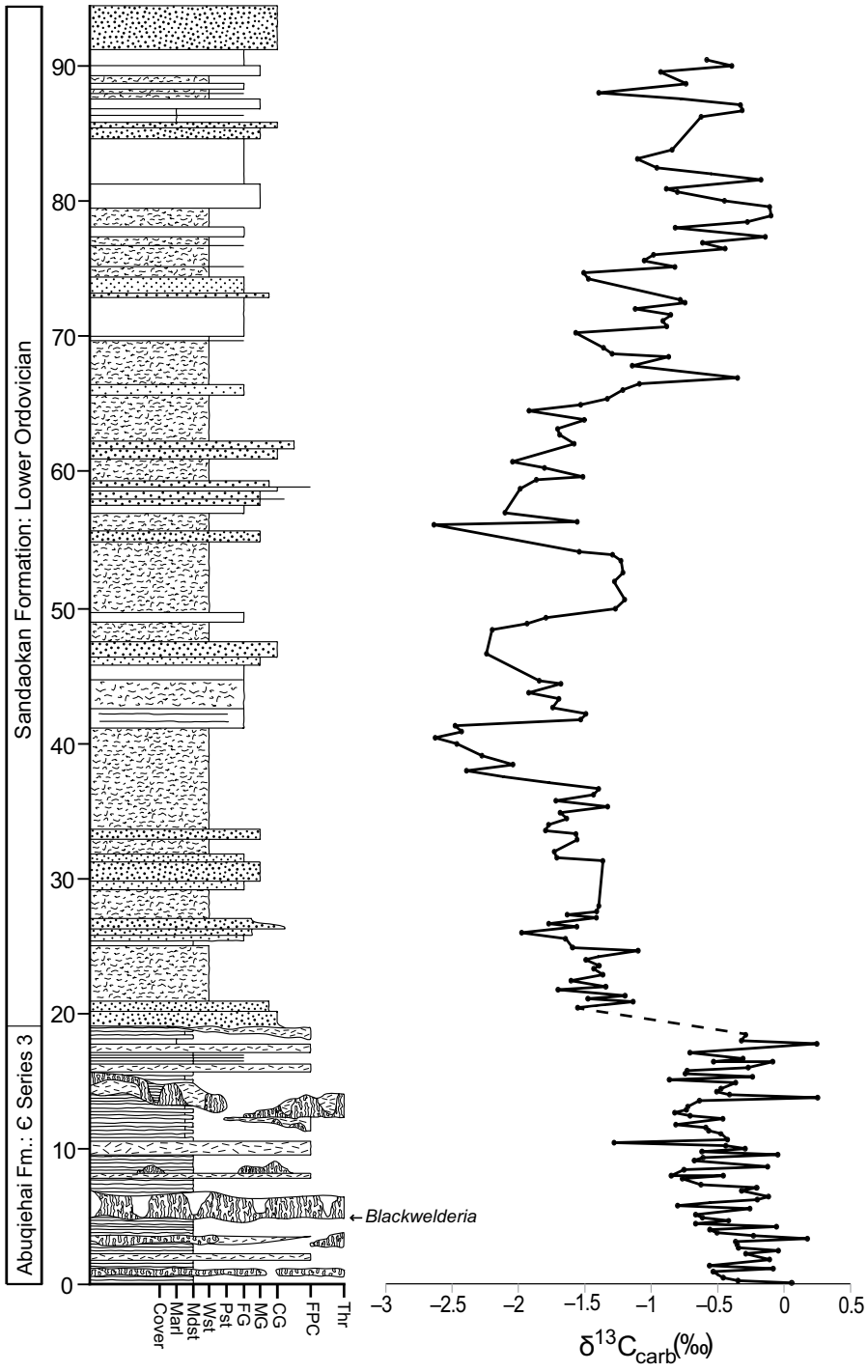

Figure 11. Carbon isotope curve for the Subaiyingou section plotted against a generalized stratigraphic column. An ~1.3‰ negative step-function jump in the curve exists across the Cambrian-Ordovician boundary just below 20 m. Abbreviations are same as in Figure 3.

variability of ~0.5‰–1‰. Strata above the Cambrian-Ordovician unconformity have a slight increase in both average $\delta^{18}O_{carb}$ and its stratigraphic variability (–6.5‰ ± 2.3‰ [1σ]), relative to those below (–8.2‰ ± 1.0‰ [1σ]; see DR Item 2 [footnote 1]); however, no correlation is observed between $\delta^{13}C_{carb}$ and $\delta^{18}O_{carb}$ data (r^2 = 0.01) and there is no indication of diagenetic alteration to the stratigraphic $\delta^{13}C_{carb}$ signal.

The carbon isotopic data for the Cambrian Subaiyingou strata show similar values (~0‰ to –0.5‰) to those of the upper part of the Cambrian Series 3 strata (Fig. 12; e.g., Buggisch et al., 2003), which, in combination with the absence of the globally recognized Steptoean positive carbon isotope excursion of the lower Furongian, indicates that these rocks can be assigned to the latest part of Cambrian Series 3.

Isotopic values in the Ordovician strata show a slight fall and then rise (Fig. 12), similar to that of Edwards and Saltzman (2014) for the lower Darriwilian. More complete data sets for the Darriwilian Stage strata in Baltoscandia (Bergström et al., 2009; Lehnert et al., 2014) and South China (Schmitz et al., 2010; Munnecke et al., 2011) reveal the presence of an ~1.5‰ positive mid-Darriwilian carbon isotope excursion. Our data are likely somewhere on the rising limb of that excursion (Fig. 12). The absolute values of our Ordovician data are similar to those of the Argentinian Precordillera (Buggisch et al., 2003); however, our values are offset higher by ~1‰ than data from western Laurentia for this interval (Edwards and Saltzman, 2014) and offset lower by ~1.5‰ from other areas of the globe (Lehnert et al., 2014), which have almost entirely positive values recorded in the full mid-Darriwilian carbon isotope excursion (Fig. 12). The source of this regional variation in $\delta^{13}C_{carb}$ remains poorly understood.

CAMBRIAN-ORDOVICIAN UNCONFORMITY AND IMPLICATIONS

Based on biostratigraphic data at the Subaiyingou section, Upper Middle Ordovician strata of the Sandaokan Formation rest directly on Cambrian Series 3 strata of the Abuqiehai Formation at 23.04 m. A trilobite sample collected from 4.53 m in the Subaiyingou section specifically assigns the age of this part of the Abuqiehai Formation to the *Blackwelderia* trilobite zone (Fig. 13). Conodonts recovered from the Ordovician Sandaokan Formation assign it to the Darriwilian Stage (Upper Middle Ordovician), equivalent to very youngest Arenig through Llanvirn of British stages.

Conodonts (Fig. 14) collected from the Subaiyingou section agree well with recently published Ordovician conodont biostratigraphy from Inner Mongolia (Wang et al., 2013a, 2013b). Conodonts recovered from the lower part of the Sandaokan Formation include *Histiodella holodentata* Ethington and Clarke, 1981, *Rhipidognathus* cf. *R. laiwuensis* Zhang *in* An et al., 1983, *Rhipidognathus* cf. *R. maggolensis* (Lee, 1976), *Plectodina* sp., *Ansella jemtlandica* (Löfgren, 1978), *Panderodus* sp., and *Scolopodus* cf. *S. flexilis* An, 1981, among other long-ranging taxa. We place the lower part of the Subaiyingou section in the *Histiodella holodentata* biozone, which is Middle

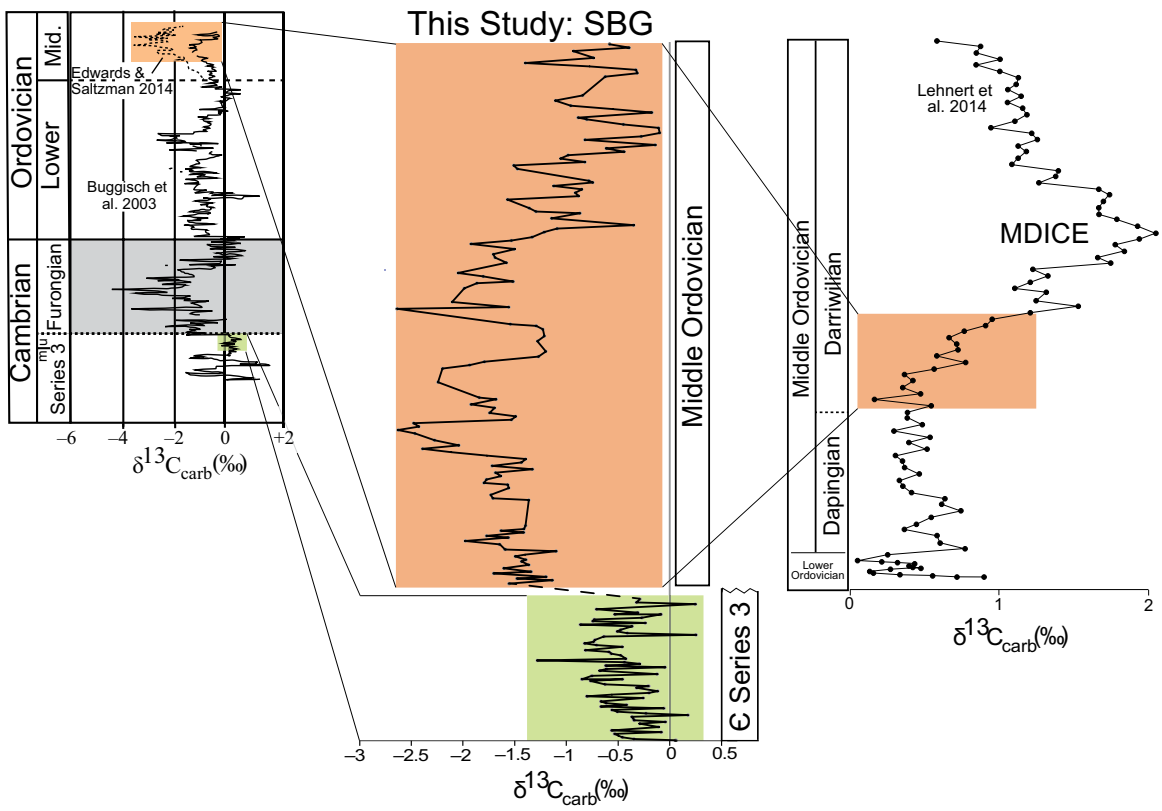

Figure 12. Correlations for the Cambrian part of the Subaiyingou (SBG) carbon isotope curve to the Buggisch et al. (2003) curve, and the Ordovician part to the Edwards and Saltzman (2014), Buggisch et al. (2003), and Lehnert et al. (2014; on right) curves. The correlation for the Cambrian is shown with green boxes, and the correlation for the Ordovician is shown with orange boxes. The middle Darriwilian carbon isotopic excursion (MDICE) is shown on the right. Old subdivisions of the Cambrian: m—Middle, u—Upper.

to Upper-Middle Darriwilian. This correlates with the upper part of the Dawangou Formation in the Tarim Basin (Zhen et al., 2011). This age for the lower part of the Sandaokan Formation may be slightly older than the age reported by Wang et al. (2013a) for the Zhuozishan and lower Kelimoli Formations. Wang et al. (2013a) placed the Zhuozishan and lower Kelimoli Formations in the *Histiodella kristinae* biozone. They defined the *Histiodella kristinae* biozone as containing *H. kristinae* Stouge, 1984 along with its probable ancestor, *H. holodentata*, for which the subjacent and globally correlated *H. holodentata* zone is named. No specimens of *H. kristinae* were recovered from samples in the Subaiyingou section, and it is difficult distinguish between the *H. holodentata* biozone and the overlying *H. kristinae* biozone with neither the occurrence of *H. kristinae* nor the presence of distinctive pectiniform species, such as *Dzikodus tablepointensis* (Stouge, 1984), *Polonodus clivosus* (Viira, 1974), or *Polonodus newfoundlandensis* (Stouge, 1984), which characterize the *H. kristinae* zone in the Tarim Basin (Zhen et al., 2011).

This biostratigraphic data at our field sites provide tight chronostratigraphic constraint on the timing and duration (~30 m.y.) of the Cambrian-Ordovician unconformity for the western margin of the North China block for comparison to other parts of the North China block and other regions globally. A Cambrian-Ordovician boundary unconformity exists in the northern margin (Daqingshan Mountain region, west of Hohhot, North China; Fig. 1A) of the North China block, where it is recorded by basal Ordovician conglomerate and arkose sandstone that rest on a highly irregular paleokarst surface (Peng et al., 2002). On the eastern margin of the North China block (Taebaeksan Basin, South Korea; Fig. 1A), it is recorded by input of siliciclastic sand into a carbonate ramp system (Kwon et al., 2006). The unconformity also exists in the northeast margin of the North China block (Dayangcha region, Jilin Province, Northeast China; Fig. 1A), which is recognized by both sedimentological and geochemical studies (Ripperdan et al., 1993; Zhang et al., 2000). A Cambrian-Ordovician unconformity also exists in other regions such as South China, Tarim, Australia, Laurentia, and Argentina (Ripperdan et al., 1992; Zhang et al., 2000; Buggisch et al., 2003; Jing et al., 2008). The unconformities in these various localities, as well as in the North China block, may have resulted in part from well-known eustatic falls, including the Late Cambrian Lange Ranch eustatic event (Miller, 1984) and an earliest Middle Ordovician event (e.g., Meng et al., 1997; Kwon et al., 2006; Haq and Schutter, 2008). The duration of these unconformities in these other parts of the North China block and elsewhere is generally brief relative to our sections, namely, latest Cambrian to earliest Ordovician, and in some cases, there may be as little as one part of a biozone missing (Table 1).

The one region from East Gondwana that records an unconformity of similar timing and magnitude to that of the western margin of the North China block is that found along the northern Indian continental margin of the Himalaya. In the Tethyan zone of the western Himalaya, the youngest Cambrian faunas found below the Cambrian-Ordovician unconformity range from latest Middle Cambrian (e.g., Spiti and Zanskar

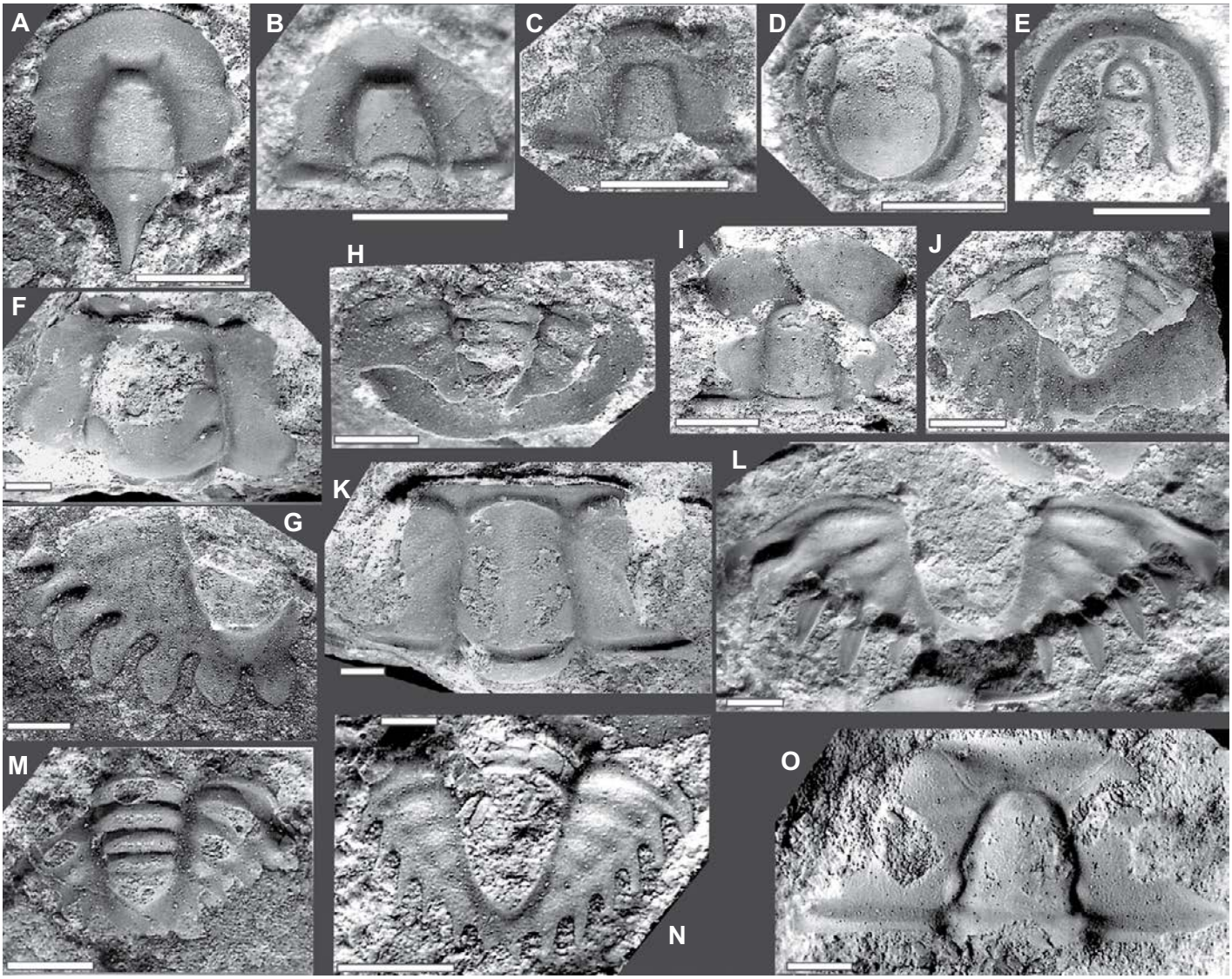

Figure 13. Representative trilobites from the *Blackwelderia tenuilimbata* zone in the upper part of the Abuqiehai Formation (Cambrian Series 3), Subaiyingou section. (A) *Cyclolorenzella distincta* Zhang, 1985, cranidium, NIGP62285. (B) *Jiulongshania rotundata* (Resser and Endo, 1937), cranidium, NIGP62278. (C) *Pingluaspis decora* (Wang and Lin, 1990), cranidium, NIGP62288. (D) *Formosagnostus formosus* Ergaliev, 1980, pygidium, NIGP62293. (E) *Formosagnostus formosus* Ergaliev, 1980, cranidium, NIGP62297. (F) *Haibowania brevis* Yuan, sp. nov., cranidium, paratype, NIGP62985–885. (G) *Haibowania brevis* Yuan, sp. nov., pygidium, holotype, NIGP62985–884. (H) *Chuangioides subaiyinggouensis* Zhang, 1985, pygidium, NIGP62411. (I) *Monkaspis neimonggolensis* Zhang, 1985, cranidium, NIGP62985–862. (J) *Monkaspis neimonggolensis* Zhang, 1985, pygidium, NIGP62985–869. (K) *Haibowania zhuozishanensis* Zhang, 1985, cranidium, NIGP62985–872. (L) *Haibowania zhuozishanensis* Zhang, 1985, pygidium, NIGP62985–876. (M) *Blackwelderia tenuilimbata* Zhou, *in* Zhou and Zheng, 1980, pygidium, NIGP62985–890. (N) *Teinistion triangulus* Yuan, sp. nov., pygidium, paratype, NIGP62985–900. (O) *Teinistion triangulus* Yuan, sp. nov., cranidium, holotype, NIGP62985–898. Scale bar is 2 mm long.

Valleys; Myrow et al., 2006a, 2006b, 2009; Peng et al., 2009) to earliest Upper Cambrian (Kashmir; Jell, 1986; Jell and Hughes, 1997). Beds overlying the unconformity in this region are no older than early Middle Ordovician in age (Myrow et al., 2006b). No Early Ordovician strata are described from the western Himalaya. Thus, the known hiatus in this region ranges from earliest Late Cambrian to early Middle Ordovician, which matches that from the western North China block, and it is distinct from those on the other margins of the North China block and other tectonostratigraphic units in adjacent areas.

The tectonic event responsible for uplift, intrusion, erosion, and deposition of coarse molasse along the northern Indian continental margin is known as the Kurgiakh (Srikantia, 1981) or Bhimphedian (Cawood et al., 2007) orogeny. The event was characterized by volcanism (Garzanti et al., 1986; Valdiya, 1997), mild metamorphism (Gaetani et al., 1985), and granitic intrusions (LeFort et al., 1986). Several workers have related this event to development of a foreland basin associated with subduction, basin closure, and accretion of an unknown terrane to the north (Garzanti et al., 1986; Gehrels

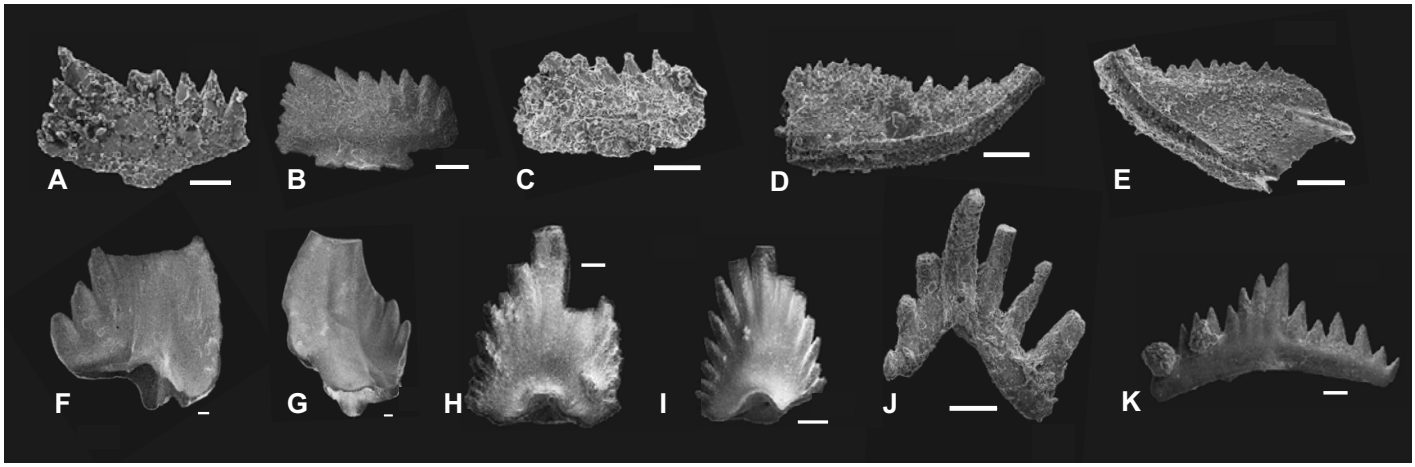

Figure 14. Selected conodonts from the Sandaokan Formation at Section SBG. Scale bar is 0.5 mm. *Histiodella holodentata* Ethington and Clarke, 1982 (A, B, and C) lateral views (NIGP161436, NIGP161437, NIGP16138). *Ansella jemtlandica* (Löfgren, 1978), (D and E) lateral views (NIGP161439, NIGP161440). *Rhipidognathus* cf. *R. maggolensis* (Lee, 1976), (F and G) posterior views (NIGP161441, NIGP161442). *Rhipidognathus* cf. *R. laiwuensis* Zhang in An et al. 1983, (H and I) posterior views. *Plectodina* sp., (J) posterior view (NIGP161443), (K) lateral view (NIGP161444).

et al., 2003), although Myrow et al. (2006b) questioned the nature and timing of the event. In any case, the event appears to have affected many areas across the northern Gondwana region (Argles et al., 1999; Gehrels et al., 2003; Kohn et al., 2004; Yin et al., 2010), including areas in Tibet (Zhu et al., 2012; Zhang et al., 2012; Liu et al., 2002; Zhou et al., 2004), Myanmar (Mitchell et al., 2012), and the Kathmandu klippe in Nepal (Gehrels et al., 2003). Although the paleogeographic relationships and distribution of the effects of this orogenic event are not well constrained, similarities between the timing and duration of the Cambrian-Ordovician unconformity in our studied strata of the western margin of the North China block suggest a link to the northern Indian margin of east Gondwana (McKenzie et al., 2011). Such a reconstructions is at odds with the previous placement of the North China block as a terrane separated from Australia by a Chilean trench–style subduction zone (Li and Powell, 2001), as an extension of the north Australian shelf (Veevers, 2000), or outboard of north Australia along with other terranes (Sibumasu, Indochina, and West Burma; Metcalfe, 2006). On the other hand, Huang et al. (2000) considered the North China block to have been an isolated block to the southwest of Antarctica. Most of these reconstructions, except Veevers' (2000) reconstruction, have the North China block as an isolated terrane, separated from the core of Gondwanaland.

TABLE 1. CAMBRIAN-ORDOVICIAN UNCONFORMITY REPORTED FROM NORTH CHINA BLOCK AND OTHER BLOCKS

References	Margins/blocks	Timing and duration of unconformity	Geological features	Geochemical features
This study	Western margin of North China block (Wuhai, Inner Mongolia)	Significant unconformity between latest Cambrian Series 3 to Upper Middle Ordovician	Ordovician sandstone unit overlying Cambrian mixed fine-siliciclastic and carbonate succession	Abrupt shift in carbon isotope values
Peng et al. (2002)	Northern margin of North China block (Baotou, Inner Mongolia)	Unconformity between Middle-Upper Cambrian and Lower Ordovician; no accurate biostratigraphy presented	Basal Ordovician conglomerate and sandstone unit overlying a paleokarst surface on Cambrian dolomitic succession	None
Ripperdan et al. (1993); Zhang et al. (1999)	Northeastern margin of North China block (Baishan, Jilin Province)	Several unconformities of different duration in the Upper Cambrian to Lower Ordovician	Subaerial exposure structures such as desiccation cracks, subaerial erosional surface, and drowning surface	Positive excursion of carbon isotope
Kwon et al. (2006)	Eastern margin of North China block (Taebaek, South Korea)	A brief unconformity between the uppermost Cambrian and lowermost Ordovician	Shoreface sandstone unit overlying middle-outer ramp carbonate unit	None
Ripperdan et al. (1992)	Australia (Black Mountain)	Several brief unconformities in Upper Cambrian and Lower Ordovician	Coincident with conodont zone boundaries	Positive excursion of carbon isotope
Zhang et al. (2000)	South China (Yichang, Hubei Province)	Several brief unconformities in Upper Cambrian and Lower Ordovician	Formation of paleokarst on the platform and input of siliciclastic sediment in the slope settings	Negative excursion of carbon isotope
Buggisch et al. (2003)	Argentina (Argentine Precordillera)	Several brief unconformities in Upper Cambrian and Lower Ordovician	Supratidal and even terrestrial (caliches) features; chert-clast breccia on erosional surface	Positive excursion of carbon isotope
Miller (1984)	Laurentia (central Texas)	An unconformity in the uppermost Cambrian: "Lange Ranch eustatic event"	Missing biozones	None
Jing et al. (2008)	Tarim block (Akesu region)	Several brief unconformities during the Upper Cambrian to Lower Ordovician	Dolomitic limestone overlying dolomitic microbial laminite	Beginning of positive excursion of carbon isotope

In Inner Mongolia, a change in detrital zircon age spectra between Cambrian and Ordovician strata, described by Darby and Gehrels (2006), supports changes in provenance associated with tectonic uplift at this time. This and the timing and duration of the hiatus associated with the Cambrian-Ordovician unconformity suggest that the North China block was part of Gondwana, and that this margin of the North China block was an along-strike continuation of the northern Indian continental margin (Fig. 15). These data are in agreement with recently published detrital zircon and trilobite biogeographic data that argue for paleogeographic continuity between the Bhutanese part of the northern Indian continental margin and the North China block (McKenzie et al., 2011). Although our lines of reasoning strongly suggest a link to Gondwana and the Bhimphedian orogeny, further studies are required to test this hypothesis.

CONCLUSIONS

Integrated sedimentological, paleontological, and geochemical investigations on the Cambrian–Ordovician succession in the Subaiyingou section, western Inner Mongolia, indicate the presence of a significant disconformity (~30 m.y. in duration) between the Cambrian and Ordovician in the western margin of the North China block. Based on trilobite and conodont data and carbon isotope chemostratigraphic correlations, the older strata (Abuqiehai Formation) at the Subaiyingou section are uppermost Cambrian Series 3 (Guzhangian), and the younger strata (Sandaokan Formation) of the Subaiyingou section are late Middle Ordovician (Darriwilian). The Cambrian Abuqiehai Formation consists mainly of limestone-shale/marlstone, flat-pebble conglomerate, and maceriate microbialite, similar to the typical facies of the inner detrital belt of Laurentia. The Ordovician Sandaokan Formation is dominated by bioturbated wackestone and quartz sandstone, which formed retrogradationally stacked parasequences during relatively long-term transgression. The lower part of the Sandaokan Formation contains the rising limb of the middle Darriwilian positive carbon isotopic excursion, which is the first record of it in the western North China block. The timing and duration of the Cambrian-Ordovician unconformity in the west North China block are comparable with those in the North India regions relative to the brief unconformity in other localities of the North China block and elsewhere, indicating a potential paleogeographic link of the North China block to the northern Indian margin of east Gondwana.

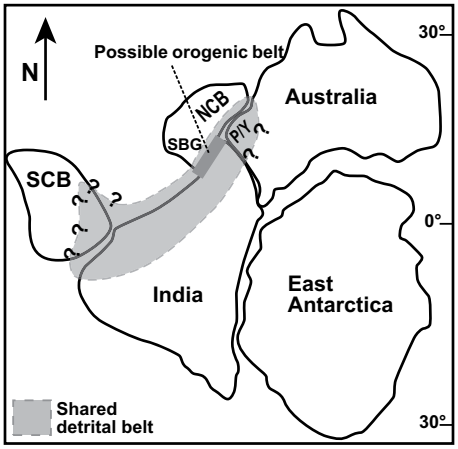

Figure 15. Paleogeographic reconstruction of east Gondwana during the latest Cambrian (modified from McKenzie et al., 2011). NCB—North China block; SBG—studied section, Subaiyingou section; SCB—South China block; P/Y—Pilbara/Yilgarn cratons. The close affinity between the modern western margin of the North China block and the northern part of the Indian craton is indicated by a shared detrital belt (McKenzie et al., 2011) and the Cambrian-Ordovician unconformity of similar timing and duration (this study).

ACKNOWLEDGMENTS

This study was supported by grants to Myrow from the National Science Foundation (EAR-1124518) and to Chen from the National Natural Science Foundation of China (41302077 and 41290260). We thank X. Zhu from Nanjing Institute of Geology and Palaeontology, Chinese Academy of Sciences, for field guidance and assistance. We thank reviewer J. Javier Álvaro, an anonymous reviewer, associate editor Brian Pratt, and editor Christian Koeberl for constructive reviews and guidance.

REFERENCES CITED

An, T.X., 1981, Recent progress in Cambrian and Ordovician conodont biostratigraphy of China, *in* Teichert, C., Liu, L., and Yin, Z.-X., eds., Paleontology in China, 1979: Geological Society of America Special Paper 187, p. 209–226.

An, T.X., Zhang, F., Xiang, W.D., Zhang, Y.Q., Xu, W.H., Zhang, H.J., Jiang, D.B., Yang, C.S., Lin, L.D., Cui, Z.T., and Yang, X.C., 1983, The Conodonts of North China and the Adjacent Regions: Beijing, Science Press, 223 p. [in Chinese with English abstract].

Argles, T.W., Prin, C.I., Foster, G.L., and Vance, D., 1999, New garnets for old? Cautionary tales from young mountain belts: Earth and Planetary Science Letters, v. 172, p. 301–309, doi:10.1016/S0012-821X(99)00209-5.

Bergström, S.M., Chen, X., Gutiérrez-Marco, J.C., and Dronov, A., 2009, The new chronostratigraphic classification of the Ordovician System and its relations to major regional series and stages and to $\delta^{13}C$ chemostratigraphy: Lethaia, v. 42, p. 97–107, doi:10.1111/j.1502-3931.2008.00136.x.

Bian, Q., Gao, S., Li, D., Ye, Z., Chang, C., and Luo, X., 2001, A study of the Kunlun-Qilian-Qinling suture system: Acta Geologica Sinica (English Edition), v. 75, p. 364–374.

Black, L.P., Kamo, S.L., Williams, I.S., Mundil, R., Davis, D.W., Korsch, R.J., and Foudoulis, C., 2003, The application of SHRIMP to Phanerozoic geochronology: A critical appraisal of four zircon standards: Chemical Geology, v. 200, p. 171–188, doi:10.1016/S0009-2541(03)00166-9.

Blakey, R.C., 2008, Gondwana paleogeography from assembly to breakup—A 500 million year odyssey, *in* Fielding, C.R., Frank, T.D., and Isbell, J.L., eds., Resolving the Late Paleozoic Ice Age in Time and Space: Geological Society of America Special Paper 441, p. 1–28.

Buggisch, W., Keller, M., and Lehnert, O., 2003, Carbon isotope record of Late Cambrian to Early Ordovician carbonates of the Argentine Precordillera: Palaeogeography, Palaeoclimatology, Palaeoecology, v. 195, p. 357–373, doi:10.1016/S0031-0182(03)00365-1.

Burchette, T.P., and Wright, V.P., 1992, Carbonate ramp depositional systems: Sedimentary Geology, v. 79, p. 3–57, doi:10.1016/0037-0738(92)90003-A.

Burrett, C., and Richardson, R., 1980, Trilobite biogeography and Cambrian tectonic models: Tectonophysics, v. 63, p. 155–192, doi:10.1016/0040-1951(80)90113-4.

Calvet, F., and Tucker, M.E., 1988, Outer ramp cycles in the Upper Muschelkalk of the Catalan Basin, northeast Spain: Sedimentary Geology, v. 57, p. 185–198, doi:10.1016/0037-0738(88)90026-7.

Cawood, P.A., Johnson, M.R.W., and Nemchin, A.A., 2007, Early Palaeozoic orogenesis along the Indian margin of Gondwana: Tectonic response to Gondwana assembly: Earth and Planetary Science Letters, v. 255, p. 70–84, doi:10.1016/j.epsl.2006.12.006.

Chen, J., 2014, Surface and subsurface reworking by storms on a Cambrian carbonate platform: Evidence from limestone breccias and conglomerates: Geologos, v. 20, p. 13–23, doi:10.2478/logos-2014-0002.

Chen, J., and Lee, H.S., 2013, Soft-sediment deformation structures in Cambrian siliciclastic and carbonate storm deposits (Shandong Province, China): Differential liquefaction and fluidization triggered by storm-wave loading: Sedimentary Geology, v. 288, p. 81–94, doi:10.1016/j.sedgeo.2013.02.001.

Chen, J., and Lee, J.-H., 2014, Current progress on the geological record of microbialites and microbial carbonates: Acta Geologica Sinica (English Edition), v. 88, p. 260–275, doi:10.1111/1755-6724.12196.

Chen, J., Chough, S.K., Chun, S.S., and Han, Z., 2009, Limestone pseudoconglomerates in the Late Cambrian Gushan and Chaomidian Formations (Shandong Province, China): Soft-sediment deformation induced by storm-wave loading: Sedimentology, v. 56, p. 1174–1195, doi:10.1111/j.1365-3091.2008.01028.x.

Chen, J., Han, Z., Zhang, X., Fan, A., and Yang, R., 2010, Early diagenetic deformation structures of the Furongian ribbon rocks in Shandong Province of China—A new perspective of the genesis of limestone conglomerates: Science China Earth Sciences, v. 53, p. 241–252, doi:10.1007/s11430-010-0010-6.

Chen, J., Chough, S.K., Han, Z., and Lee, J.-H., 2011, An extensive erosion surface of a strongly deformed limestone bed in the Gushan and Chaomidian Formations (late Middle Cambrian to Furongian), Shandong Province, China: Sequence-stratigraphic implications: Sedimentary Geology, v. 233, p. 129–149, doi:10.1016/j.sedgeo.2010.11.002.

Chen, J., Chough, S.K., Lee, J.-H., and Han, Z., 2012, Sequence-stratigraphic comparison of the upper Cambrian Series 3 to Furongian succession between the Shandong region, China, and the Taebaek area, Korea: High variability of bounding surfaces in an epeiric platform: Geosciences Journal, v. 16, p. 357–379, doi:10.1007/s12303-012-0040-5.

Chen, J., Lee, J.-H., and Woo, J., 2014, Formative mechanisms, depositional processes, and geological implications of Furongian (Late Cambrian) reefs in the North China Platform: Palaeogeography, Palaeoclimatology, Palaeoecology, v. 414, p. 246–259, doi:10.1016/j.palaeo.2014.09.004.

Chough, S.K., Kwon, S.T., Ree, J.H., and Choi, D.K., 2000, Tectonic and sedimentary evolution of the Korean peninsula: A review and new view: Earth-Science Reviews, v. 52, p. 175–235, doi:10.1016/S0012-8252(00)00029-5.

Chough, S.K., Lee, H.S., Woo, J., Chen, J., Choi, D.K., Lee, S.-b., Kang, I., Park, T.-Y., and Han, Z., 2010, Cambrian stratigraphy of the North China Platform: Revisiting principal sections in Shandong Province, China: Geosciences Journal, v. 14, p. 235–268, doi:10.1007/s12303-010-0029-x.

Darby, B.J., and Gehrels, G., 2006, Detrital zircon reference for the North China block: Journal of Asian Earth Sciences, v. 26, p. 637–648, doi:10.1016/j.jseaes.2004.12.005.

Darby, B.J., and Ritts, B.D., 2002, Mesozoic contractional deformation in the middle of the Asian tectonic collage: The intraplate Western Ordos fold-thrust belt, China: Earth and Planetary Science Letters, v. 205, p. 13–24, doi:10.1016/S0012-821X(02)01026-9.

Droser, M.L., and Bottjer, D.J., 1986, A semiquantitative field classification of ichnofabric: Journal of Sedimentary Petrology, v. 56, p. 558–559, doi:10.1306/212F89C2-2B24-11D7-8648000102C1865D.

Dumas, S., Arnott, R.W.C., and Southard, J.B., 2005, Experiments on oscillatory-flow and combined-flow bed forms; implications for interpreting parts of the shallow-marine sedimentary record: Journal of Sedimentary Research, v. 75, p. 501–513, doi:10.2110/jsr.2005.039.

Edwards, C.T., and Saltzman, M.R., 2014, Carbon isotope $\delta^{13}C$ stratigraphy of the Lower–Middle Ordovician (Tremadocian–Darriwilian) in the Great Basin, western United States: Implications for global correlation: Palaeogeography, Palaeoclimatology, Palaeoecology, v. 399, p. 1–20, doi:10.1016/j.palaeo.2014.02.005.

Ergaliev, G.K., 1980, Middle and Upper Cambrian trilobites from Malyi Karatau: Nauka, Alma-Ata, 208 p. [in Russian].

Ethington, R.L., and Clarke, D.L., 1981, Lower and Middle Ordovician conodonts from the Ibex area, western Millard County, Utah: Brigham Young University Geology Studies, v. 28, part 2, p. 1–155.

Feng, Z., Peng, Y., Jin, Z., and Bao, Z., 2002, Lithofacies palaeogeography of the Late Cambrian in China: Journal of Palaeogeography, v. 4, p. 1–10 [in Chinese with English abstract].

Fergusson, C.L., Henderson, R.A., Fanning, C.M., and Withnall, I.W., 2007, Detrital zircon ages in Neoproterozoic to Ordovician siliciclastic rocks, northeastern Australia: Implications for the tectonic history of the East Gondwana continental margin: Journal of the Geological Society of London, v. 164, p. 215–225, doi:10.1144/0016-76492005-136.

Gaetani, M., Garzanti, E., and Jadoul, F., 1985, Main Structural elements of Zanskar, NW Himalaya (India): Rendiconti della Società Geologica Italiana, v. 8, p. 3–8.

Garzanti, E., Casnedi, R., and Jadoul, F., 1986, Sedimentary evidence of a Cambro–Ordovician orogenic event in the Northwestern Himalaya: Sedimentary Geology, v. 48, p. 237–265, doi:10.1016/0037-0738(86)90032-1.

Gehrels, G.E., DeCelles, P.G., Martin, A., Ojha, T.P., Pinhassi, G., and Upreti, B.N., 2003, Initiation of the Himalayan orogen as an early Paleozoic thin-skinned thrust belt: GSA Today, v. 13, no. 9, p. 4–9, doi:10.1130/1052-5173(2003)13<4:IOTHOA>2.0.CO;2.

Goodge, J.W., Williams, I.S., and Myrow, P., 2004, Provenance of Neoproterozoic and lower Paleozoic siliciclastic rocks of the central Ross orogen, Antarctica: Detrital record of rift-, passive-, and active-margin sedimentation: Geological Society of America Bulletin, v. 116, p. 1253–1279, doi:10.1130/B25347.1.

Haq, B.U., and Schutter, S.R., 2008, A chronology of Paleozoic sea-level changes: Science, v. 322, p. 64–68, doi:10.1126/science.1161648.

Heckel, P.H., 1972, Possible inorganic origin for stromatactis in calcilutite mounds in the Tully Limestone, Devonian of New York: Journal of Sedimentary Petrology, v. 42, p. 7–18.

Huang, B., Zhu, R., Otofuji, Y., and Yang, Z., 2000, The early Paleozoic paleogeography of the North China block and the other major blocks of China: Chinese Science Bulletin, v. 45, p. 1057–1065, doi:10.1007/BF02887174.

Jell, P.A., 1986, An early Late Cambrian trilobite faunule from Kashmir: Geological Magazine, v. 123, p. 487–492, doi:10.1017/S001675680003507X.

Jell, P.A., and Hughes, N.C., 1997, Himalayan Cambrian Trilobites: Special Papers in Palaeontology 58, 113 p.

Jeppsson, L., and Anehus, R., 1995, A buffered formic acid technique for conodont extraction: Journal of Paleontology, v. 69, p. 790–794.

Jing, X., Deng, S., Zhao, Z., Lu, Y., and Zhang, S., 2008, Carbon isotope composition and correlation across the Cambrian-Ordovician boundary in Kalpin region of the Tarim Basin, China: Science in China Series D: Earth Science, v. 51, p. 1317–1329.

Keller, M., 1997, Evolution and sequence stratigraphy of an Early Devonian carbonate ramp, Cantabrian Mountains, northern Spain: Journal of Sedimentary Research, v. 67, p. 638–652.

Kohn, M.J., Widland, M.S., Parkinson, C.D., and Upreti, B.N., 2004, Miocene faulting at plate tectonic velocity in the Himalaya of central Nepal: Earth and Planetary Science Letters, v. 228, p. 299–310, doi:10.1016/j.epsl.2004.10.007.

Kwon, Y.K., Chough, S.K., Choi, D.K., and Lee, D.J., 2006, Sequence stratigraphy of the Taebaek Group (Cambrian–Ordovician), mideast Korea: Sedimentary Geology, v. 192, p. 19–55, doi:10.1016/j.sedgeo.2006.03.024.

Lee, H.S., and Chough, S.K., 2011, Depositional processes of the Zhushadong and Mantou Formations (Early to Middle Cambrian), Shandong Province, China: Roles of archipelago and mixed carbonate–siliciclastic sedimentation on cycle genesis during initial flooding of the North China Platform: Sedimentology, v. 58, p. 1530–1572, doi:10.1111/j.1365-3091.2011.01225.x.

Lee, H.Y., 1976, Conodonts from the Maggol Formation (Lower Ordovician), Kangwondo, South Korea: Journal of the Geological Society of Korea, v. 12, p. 151–182.

Lee, J.-H., Chen, J., and Chough, S.K., 2010, Paleoenvironmental implications of an extensive maceriate microbialite bed in the Furongian Chaomidian Formation, Shandong Province, China: Palaeogeography, Palaeoclimatology, Palaeoecology, v. 297, p. 621–632, doi:10.1016/j.palaeo.2010.09.012.

Lee, J.-H., Chen, J., and Chough, S.K., 2012, Demise of an extensive biostromal microbialite in the Furongian (Late Cambrian) Chaomidian Formation, Shandong Province, China: Geosciences Journal, v. 16, p. 275–287, doi:10.1007/s12303-012-0027-2.

Lee, J.-H., Chen, J., Choh, S.-J., Lee, D.-J., Han, Z., and Chough, S.K., 2014, Furongian (Late Cambrian) sponge–microbial maze-like reefs in the North China Platform: Palaios, v. 29, p. 27–37, doi:10.2110/palo.2013.050.

LeFort, P., Debon, F., Pêcher, A., Sonet, J., and Vidal, P., 1986, The 500 Ma magmatic event in Alpine southern Asia, a thermal episode at Gondwana scale: Sciences de la Terre, v. 47, p. 191–209.

Lehnert, O., Meinhold, G., Wu, R., Calner, M., and Joachimski, M.M., 2014, $\delta^{13}C$ chemostratigraphy in the upper Tramadocian through lower Katian (Ordovician) carbonate succession of the Siljan district, central Sweden: Estonian Journal of Earth Sciences, v. 63, p. 277–286.

Li, X., and Droser, M.L., 1997, The nature and distribution of Cambrian shell concentrations: Evidence from the Great Basin, CA, NV, UT: Palaios, v. 12, p. 111–126, doi:10.2307/3515301.

Li, Z.X., and Powell, C.M., 2001, An outline of the palaeogeographic evolution of the Australasian region since the beginning of the Neoproterozoic: Earth-Science Reviews, v. 53, p. 237–277, doi:10.1016/S0012-8252(00)00021-0.

Lin, C., Yang, Q., Li, S., and Li, Z., 1991, Sedimentary characteristics of the early Paleozoic deep water gravity flow systems and basin filling style in the Helan aulacogen: Northwest China: Geoscience, v. 5, p. 252–263 [in Chinese with English abstract].

Liu, W.C., Liang, D.Y., Wang, K.Y., Zhou, Z.G., Li, G.B., and Zhang, X.X., 2002, The discovery of the Ordovician and its significance in the Kangmar area, southern Tibet: Earth Science Frontiers, v. 9, p. 247–248 [in Chinese with English abstract].

Lochman-Balk, C., 1971, The Cambrian of the craton of the United States, *in* Holland, C.H., ed., Cambrian of the New World: New York, New York, John Wiley and Sons, p. 79–168.

Löfgren, A., 1978, Arenigian and Llanvirnian conodonts from Jämtland, northern Sweden: Fossils and Strata, no. 13, 129 p.

Ludwig, K.R., 2001, Eliminating mass-fractionation effects on U-Pb isochron ages without doubles-spiking of Pb: Geochimica et Cosmochimica Acta, v. 65, p. 3139–3145, doi:10.1016/S0016-7037(01)00637-8.

Markello, J.R., and Read, J.F., 1981, Carbonate ramp-to-deeper shale shelf transitions of an Upper Cambrian intrashelf basin, Nolichucky Formation, Southwest Virginia Appalachians: Sedimentology, v. 28, p. 573–597.

McKenzie, N.R., Hughes, N.C., Myrow, P.M., Choi, D.K., and Park, T.Y., 2011, Trilobites and zircons link North China with the Eastern Himalaya during the Cambrian: Geology, v. 39, p. 591–594, doi:10.1130/G31838.1.

Meert, J.G., and Lieberman, B.S., 2008, The Neoproterozoic assembly of Gondwana and its relationship to the Ediacaran–Cambrian radiation: Gondwana Research, v. 14, p. 5–21, doi:10.1016/j.gr.2007.06.007.

Meng, X., Ge, M., and Tucker, M.E., 1997, Sequence stratigraphy, sea-level changes and depositional systems in the Cambro-Ordovician of the North China carbonate platform: Sedimentary Geology, v. 114, p. 189–222, doi:10.1016/S0037-0738(97)00073-0.

Metcalfe, I., 2006, Palaeozoic and Mesozoic tectonic evolution and palaeogeography of East Asian crustal fragments; the Korean Peninsula in context: Gondwana Research, v. 9, p. 24–46, doi:10.1016/j.gr.2005.04.002.

Meyerhoff, A.A., Kamen-Kaye, M., Chen, C., and Taner, I., 1991, China—Stratigraphy, Paleogeography, and Tectonics: Dordrecht, Netherlands, Kluwer Academic Publishers, 188 p.

Miller, J.F., 1984, Cambrian and earliest Ordovician conodont evolution, biofacies, and provincialism, *in* Clark, D.L., ed., Conodont Biofacies and Provincialism: Geological Society of America Special Paper 196, p. 43–68.

Mitchell, A., Chung, S.-L., Oo, T., Lin, T.-H., and Hung, C.-H., 2012, Zircon U-Pb ages in Myanmar: Magmatic-metamorphic events and the closure of a neo-Tethys ocean?: Journal of Asian Earth Sciences, v. 56, p. 1–23, doi:10.1016/j.jseaes.2012.04.019.

Morrow, J.R., and Webster, G.D., 1989, A cryogenic density separation technique for conodont and heavy mineral separations: Journal of Paleontology, v. 63, p. 953–955.

Mount, J.F., and Kidder, D., 1993, Combined flow origin of edgewise intraclast conglomerates: Sellick Hill Formation (Lower Cambrian), South Australia: Sedimentology, v. 40, p. 315–329, doi:10.1111/j.1365-3091.1993.tb01766.x.

Munnecke, A., Zhang, Y., Liu, X., and Cheng, J., 2011, Stable carbon isotope stratigraphy in Ordovician of South China: Palaeogeography, Palaeoclimatology, Palaeoecology, v. 307, p. 17–43, doi:10.1016/j.palaeo.2011.04.015.

Myrow, P.M., 1990, A new graph for understanding colors of mudrocks and shales: Journal of Geological Education, v. 38, p. 16–20.

Myrow, P.M., 1992, Bypass-zone tempestite facies model and proximality trends for an ancient muddy shoreline and shelf: Journal of Sedimentary Research, v. 62, p. 99–115.

Myrow, P.M., and Southard, J.B., 1991, Combined-flow model for vertical stratification sequences in shallow marine storm-deposited beds: Journal of Sedimentary Petrology, v. 61, p. 202–210.

Myrow, P.M., and Southard, J.B., 1996, Tempestite deposition: Journal of Sedimentary Research, v. 66, p. 875–887.

Myrow, P.M., Taylor, J.F., Miller, J.F., Ethington, R.L., Ripperdan, R.L., and Allen, J., 2003, Fallen arches: Dispelling myths concerning Cambrian and Ordovician paleogeography of the Rocky Mountain region: Geological Society of America Bulletin, v. 115, p. 695–713, doi:10.1130/0016-7606(2003)115<0695:FADMCC>2.0.CO;2.

Myrow, P.M., Tice, L., Archuleta, B., Clark, B., Taylor, J.F., and Ripperdan, R.L., 2004, Flat-pebble conglomerate: Its multiple origins and relationship to metre-scale depositional cycles: Sedimentology, v. 51, p. 973–996, doi:10.1111/j.1365-3091.2004.00657.x.

Myrow, P.M., Thompson, K.R., Hughes, N.C., Paulsen, T.S., Sell, B.K., and Parcha, S.K., 2006a, Cambrian stratig-

raphy and depositional history of the northern Indian Himalaya, Spiti Valley, north-central India: Geological Society of America Bulletin, v. 118, p. 491–510, doi: 10.1130/B25828.1.

Myrow, P.M., Snell, K.E., Hughes, N.C., Paulsen, T.S., Heim, N.A., and Parcha, S.K., 2006b, Cambrian depositional history of the Zanskar Valley region of the Indian Himalaya: Tectonic implications: Journal of Sedimentary Research, v. 76, p. 364–381, doi:10.2110/jsr.2006.020.

Myrow, P.M., Hughes, N.C., Searle, M.P., Fanning, C.M., Peng, S.-C., and Parcha, S.K., 2009, Stratigraphic correlation of Cambrian–Ordovician deposits along the Himalaya: Implications for the age and nature of rocks in the Mt. Everest region: Geological Society of America Bulletin, v. 121, p. 323–332, doi:10.1130/B26384.1.

Myrow, P.M., Hughes, N.C., Goodge, J.W., Fanning, C.M., Williams, I.S., Peng, S., Bhargava, O.N., Parcha, S.K., and Pogue, K.R., 2010, Extraordinary transport and mixing of sediment across Himalayan central Gondwana during the Cambrian-Ordovician: Geological Society of America Bulletin, v. 122, p. 1660–1670, doi:10.1130/B30123.1.

Myrow, P.M., Taylor, J.F., Runkel, A.C., and Ripperdan, R.L., 2012, Mixed siliciclastic-carbonate upward-deepening cycles of the Upper Cambrian inner detrital belt of Laurentia: Journal of Sedimentary Research, v. 82, p. 216–231, doi:10.2110/jsr.2012.20.

Overstreet, R.B., Oboh-Ikuenobe, F.E., and Gregg, J.M., 2003, Sequence stratigraphy and depositional facies of Lower Ordovician cyclic carbonate rocks, southern Missouri, U.S.A.: Journal of Sedimentary Research, v. 73, p. 421–433, doi:10.1306/112002730421.

Peng, S., Hughes, N.C., Heim, N.A., Sell, B.K., Zhu, X., Myrow, P.M., and Parcha, S.K., 2009, Cambrian trilobites from the Parahio and Zanskar Valleys, Indian Himalaya: Journal of Paleontology, v. 83, p. 1–95, doi: 10.1666/08-129.1.

Peng, X., Cheng, L., Xu, Z., and Liu, Z., 2002, An important sequence interface between the Cambrian and the Ordovician in Daqingshan, Inner Mongolia: Geological Review, v. 48, p. 54–58 [in Chinese with English abstract].

Resser, C.E., and Endo, R., 1937, Description of fossils, *in* Endo, R., and Resser, C.E., eds., The Sinian and Cambrian formations and fossils of southern Manchouria: Bulletin of the Manchurian Science Museum, v. 1, p. 103–309.

Ripperdan, R.L., Magaritz, M., Nicoll, R.S., and Shergold, J.H., 1992, Simultaneous changes in carbon isotopes, sea level, and conodont biozones within the Cambrian–Ordovician boundary interval at Black Mountain, Australia: Geology, v. 20, p. 1039–1042.

Ripperdan, R.L., Magaritz, M., Kirschvink, J.L., 1993, Carbon isotope and magnetic polarity evidence for non-depositional events within the Cambrian-Ordovician boundary section at Dayangcha, Jilin Province, China: Geological Magazine, v. 130, p. 443–452.

Rubin, D.M., and Friedman, G.M., 1977, Intermittently emergent shelf carbonates: An example from the Cambro-Ordovician of eastern New York State: Sedimentary Geology, v. 19, p. 81–106, doi:10.1016/0037-0738(77)90026-4.

Runkel, A.C., McKay, R.M., Cowan, C.A., Miller, J.F., and Taylor, J.F., 2012, The Sauk megasequence in the cratonic interior of North America: Interplay between a fully developed inner detrital belt and the central great American carbonate bank, *in* Derby, J.R., Fritz, R.D., Longacre, S.A., Morgan, W.A., and Sternbach, C.A., eds., The Great American Carbonate Bank: The Geology and Economic Resources of the Cambrian–Ordovician Sauk Megasequence of Laurentia: American Association of Petroleum Geologists Memoir 98, p. 1001–1011.

Saltzman, M.R., Runnegar, B., and Lohmann, K.C., 1998, Carbon isotope stratigraphy of Upper Cambrian (Steptoean Stage) sequences of the eastern Great Basin: Record of a global oceanographic event: Geological Society of America Bulletin, v. 110, p. 285–297, doi:10.1130/0016-7606(1998)110<0285:CISOUC>2.3.CO;2.

Sanders, D., and Hofling, R., 2000, Carbonate deposition in mixed siliciclastic-carbonate environments on top of an orogenic wedge (Late Cretaceous, Northern Calcareous Alps, Austria): Sedimentary Geology, v. 137, p. 127–146, doi:10.1016/S0037-0738(00)00084-1.

Schmitz, B., Bergström, S.M., and Wang, X., 2010, The middle Darriwilian (Ordovician) $\delta^{13}C$ excursion (MDICE) discovered in the Yangtze Platform succession in China: Implications of its first recorded occurrences outside Baltoscandia: Journal of the Geological Society of London, v. 167, p. 249–259, doi:10.1144/0016-76492009-080.

Shapiro, R.S., and Awramik, S.M., 2006, *Favosamaceria cooperi* new group and form: A widely dispersed, time-restricted thrombolite: Journal of Paleontology, v. 80, p. 411–422, doi:10.1666/0022-3360(2006)80[411:FCNGAF]2.0.CO;2.

Srikantia, S.V., 1981, The lithostratigraphy, sedimentation and structure of Proterozoic–Phanerozoic formations of Spiti basin in the higher Himalaya of Himachal Pradesh, India, *in* Sinha, A.K., and Nautiyal, S.P., ed., Contemporary Geoscientific Researches in India (a Commemorative Volume in Honour of S.P. Nautiyal): Dehra Dun, India, Bishen Singh Mahendra Pal Singh, p. 31–48.

Stouge, S.S., 1984, Conodonts of the Middle Ordovician Table Head Formation, western Newfoundland: Fossils Strata, no. 16, 145 p.

Sun, G., and Liu, J., 1983, Helan aulacogen and front basin and their evolution: Oil and Gas Geology, v. 4, p. 236–245 [in Chinese with English abstract].

Valdiya, K.S., 1997, Proterozoic sedimentation and Pan-African geodynamic development in the Himalaya, the northern frontier of east Gondwanaland: Gondwana Research, v. 1, p. 3–9, doi:10.1016/S1342-937X(05)70002-2.

Veevers, J.J., 2000, Billion-Year Earth History of Australia and Neighbours in Gondwanaland: Sydney, Australia, Gemoc Press, 400 p.

Veevers, J.J., 2004, Gondwanaland from 650–500 Ma assembly through 320 Ma merger in Pangea to 185–100 Ma breakup: Supercontinental tectonics via stratigraphy and radiometric dating: Earth-Science Reviews, v. 68, p. 1–132, doi:10.1016/j.earscirev.2004.05.002.

Viira, V., 1974, Ordovician Conodonts of the East Baltic: Geological Institute of the Academy of Sciences of the Estonian S.S.R., "Valgus", Tallinn, 142 p. [in Russian].

Wang, H., and Lin, T., 1990, The late Changhsian and early Kushanian trilobites of Xuecheng County, Shandong Province: Journal of Nanjing University, Earth Sciences, v. 2, p. 116–122 [in Chinese with English abstract].

Wang, Z., Bergström, S.M., Zhen, Y.Y., Chen, X., and Zhang, Y.-D., 2013a, On the integration of Ordovician conodont and graptolite biostratigraphy: New examples from Gansu and Inner Mongolia in China: Alcheringa, v. 37, p. 510–528, doi:10.1080/03115518.2013.805491.

Wang, Z., Bergström, S., Zhen, Y., Zhang, Y., Wu, R., and Chen, Q., 2013b, Ordovician conodonts from Dashimen, Wuhai in Inner Mongolia, and the significance of the discovery of the *Histiodella* fauna: Acta Micropalaeontologica Sinica, v. 30, p. 323–343 [in Chinese with English abstract].

Williams, I., 1998, U-Th-Pb geochronology by ion microprobe: Reviews in Economic Geology, v. 7, p. 1–35.

Yin, A., Dubey, C.S., Kelty, T.K., Webb, A.A.G., Harrison, T.M., Chou, C.Y., and Célérier, J., 2010, Geologic correlation of the Himalayan orogen and Indian craton: Part 2. Structural geology, geochronology, and tectonic evolution of the Eastern Himalaya: Geological Society of America Bulletin, v. 122, p. 360–395, doi:10.1130/B26461.1.

Zhang, J., 1985, New materials of the early Gushanian trilobites in Zhuozishan district, Nei Monggol Zizhiqu (Autonomous region): Bulletin of Tianjin Institute of Geology and Mineral Resources, v. 13, p. 111–120 [in Chinese with English abstract].

Zhang, J., Wang, H., and Li, G., 1999, Study on sequence-stratigraphy and chemostratigraphy of the Upper Cambrian Fengshan Formation-Lower Ordovician Yehli Formation at Dayangcha (Jilin): Journal of Stratigraphy, v. 23, p. 81–106 [in Chinese with English Abstract].

Zhang, J.-M., Wang, H.-F., and Li, G.-X., 2000, Sequence stratigraphic correlation and eustatic events from latest Cambrian to early Early Ordovician between North China and Yangtze platforms: Journal of Stratigraphy, v. 24, p. 359–369 [in Chinese with English abstract].

Zhang, Z.M., Dong, X., Santosh, M., Liu, F., Wang, W., Yiu, F., He, Z.Y., and Shen, K., 2012, Petrology and geochronology of the Namche Barwa complex in the eastern Himalayan syntaxis, Tibet: Constraints on the origin and evolution of the north-eastern margin of the Indian craton: Gondwana Research, v. 21, p. 123–137, doi:10.1016/j.gr.2011.02.002.

Zhen, Y., Wang, Z., Zhang, Y., Bergström, S.M., Percival, I.G., and Cheng, J., 2011, Middle to Late Ordovician conodonts from the Dawangou section, Kalpin area of the Tarim Basin, northwestern China: Records of the Australian Museum, v. 63, p. 203–266, doi:10.3853/j.0067-1975.63.2011.1586.

Zhou, Z., and Zheng, Z., 1980, New data on the Upper Cambrian from the Helan Mountains: Bulletin of the Chinese Academy of Geological Sciences, v. 1, p. 60–77 [in Chinese with English abstract].

Zhou, Z.G., Liu, W.C., and Liang, D.Y., 2004, Discovery of the Ordovician and its basal conglomerate in the Kangmar area, southern Tibet—With a discussion of the relation of the sedimentary cover and unifying basement in the Himalayas: Geological Bulletin of China, v. 23, p. 655–663 [in Chinese with English abstract].

Zhu, D.C., Zhao, Z.D., Niu, Y.L., Dilek, Y., Wang, Q., Ji, W.H., Dong, G.C., Sui, Q.L., Liu, Y.S., Yuan, H.L., and Mo, X.X., 2012, Cambrian bimodal volcanism in the Lhasa terrane, southern Tibet: Record of an early Paleozoic Andean-type magmatic arc in the Australian proto-Tethyan margin: Chemical Geology, v. 328, p. 290–308, doi:10.1016/j.chemgeo.2011.12.024.

Science Editor: Christian Koeberl
Associate Editor: Brian R. Pratt

Manuscript Received 28 October 2014
Revised Manuscript Received 29 December 2014
Manuscript Accepted 6 February 2015

Printed in the USA